University of Saskatchewan
Subatomic Physics Internal Report

SPIR 148

Bethe-Heitler Pair Spectrometer

Rob Pywell

November 2015, Last Update: August 30, 2016

Abstract

This report details the performance of the circular pole dipole magnet to be used as an electron-positron pair spectrometer for the Bethe-Heitler experiment at HIGS. The report describes the codes used to determine the expected performance of the spectrometer. Note that many changes have occurred in the design and the functionality of the code over the life of this project. Therefore this report is written in somewhat of a narrative style detailing our design choices as they occurred. This report should therefore be considered a living document.

Contents

1 Introduction

A GEANT4 simulation has been built to model the pair spectrometer to be used by the proposed experiment to measure the Bethe-Heitler pair production asymmetries [1]. This will be described later in the report. However, in the initial stages of the design this simulation was not developed to a level that was useful in describing the optical properties of the spectrometer. Some of these limitations had to do the the limited field map of the spectrometer we had available, Therefore in the initial stages a simpler approach was used were only the magnetic field was simulated.

To do this we have resurrected the old MIT magnet design code RAYTRACE [3] to help with finalizing the design with respect to the location of the target and the location of the focal plane. RAYTRACE solves the equations of motion of charged particles subject to the Lorentz force through electric and magnetic fields defined by parameterizations for various magnet geometries. The equations of motion are solved by step-by-step numerical integration. RAYTRACE does assume the particles move in a vacuum so the GEANT4 simulation will be necessary to understand scattering effects in the final set-up.

The advantage of using RAYTRACE in the initial design was primarily because RAYTRACE uses a parameterization of the magnetic field that is better able to simulate the magnetic field in three dimensions. The field map of the magnet we have is only in two dimensions in the central plane of the magnet. RAYTRACE was then able to inform our design for the implementation of the magnetic field in GEANT4.

2 RAYTRACE Ray Optics

We have used the measured field map [2] to parametrize the magnetic field as a function of distance through the magnet, and to locate the Effective Field Boundary (EFB). This parameterization is in a form needed by RAYTRACE. The EFB is defined as the position of a sharp magnetic field cut-off that has the same field integral as the real distribution when the integral is performed along a straight line. The beam optics of a dipole magnet, such as we have here, depend critically on the location of the EFB. The actual magnetic field as a function of distance is described by a parameterization relative to the EFB. In the absence of a background magnetic field the field, in the central plane of the magnet, is described by

$$B_y = \frac{B_0}{1 + e^S} \tag{1}$$

where $S = c_0 + c_1 s + c_2 s^2 + c_3 s^3 + c_4 s^4 + c_5 s^5$ and $s = \frac{z}{D}$, where z is the distance from the EFB, D is the magnet pole gap, and B_0 is the uniform field in the magnet. It is known that the shape of the field profile described by the polynomial S is a second order effect in the optics of the magnet. Much more important is having the location of the EFB correct. The field description above is for a non-curved pole face. RAYTRACE will calculate the correction to the field for a curved pole face. Our magnet has a curved pole face and the field measurements are for the real-world curved pole face. Investigations using RAYTRACE with straight and curved pole faces show that for our magnet the difference between the EFB positions for straight and circular pole faces is smaller than our uncertainty in extracting the

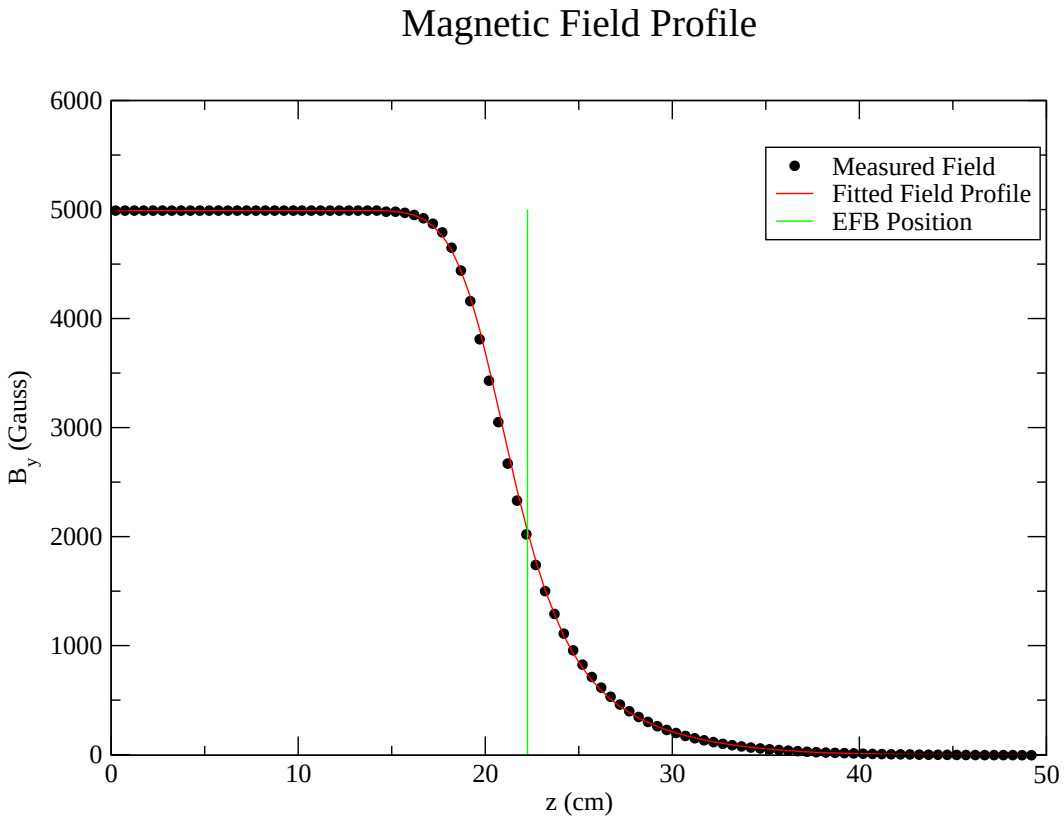

Figure 1: Magnetic field map of the circular pole pair spectrometer. The filled circles are the measured fields as a function of distance (z) along a radius from the center ($z = 0$). The red line is the fit to obtain the coefficients of the field profile. The green vertical line shows the position of the effective field boundary (EFB).

EFB position from the measurements. Therefore we have simply fitted the measured field map to find the EFB position and the coefficients of S. The result are: The EFB is 22.26 cm from the circular pole center (the radius of the circular pole is 20.00 cm). The coefficients are

$$c_0 = 0.35, c_1 = 2.71, c_2 = -0.94, c_3 = 0.27, c_4 = -0.027, c_5 = 0.0009.$$

The magnetic field profile is shown in figure 1.

3 Focal Plane

Using the parameters for the field profile found above, RAYTRACE was used to establish the position of the focal plane. The target position was initially chosen to be 20.0 cm from the EFB (or 42.26 cm from the magnet center). This initial choice was relatively arbitrary. It located the target at a distance of 3.32 cm from the outside of the magnet yoke. Rays were traced with electron momenta 25.0 MeV/c to 35.0 MeV/c. The uniform magnetic field field in the center of the dipole was adjusted so that 30.0 MeV/c emerged at right angles to the

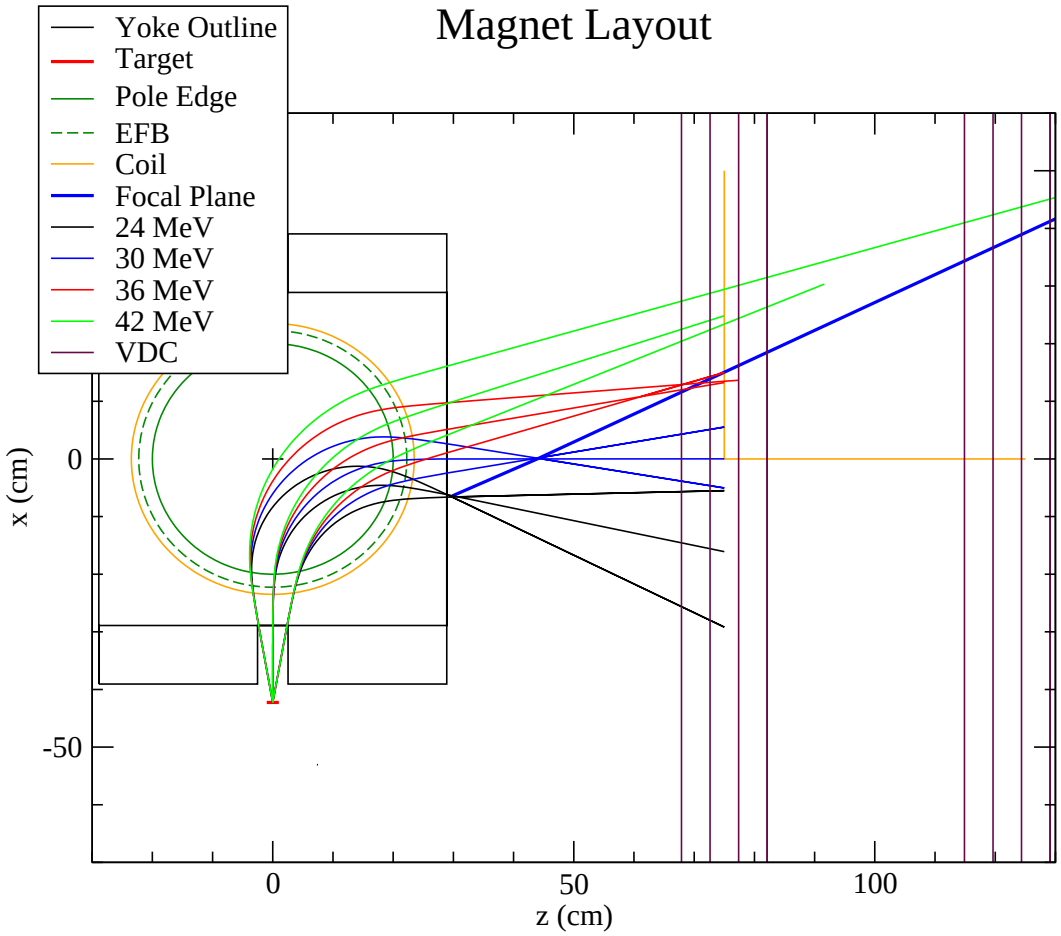

Figure 2: The layout of the magnet showing the locations of the target and the focal plane. All dimensions shown are in cm and are referenced to the center of the circular pole. The focal plane is shown only on one side. The blue line show the focal plane located by fit to the focal points corresponding the the electron momenta 25, 27.5, 30, 32.5 and 35 MeV/c.

initial beam direction. That magnetic field is 0.456 T. The focal plane was established by finding the intersection of rays emerging from the target at different angles for each energy. The resulting layout is shown in figure 2.

We have chosen to represent the focal plane in a coordinate system centered at the focal point for a 30 MeV/c electron. The Z-axis passes through the center of the circular pole of the magnet. A detail of the focal plane is shown in figure 3.

A straight line fit to the focal plane shows a good fit with the function

$$x = 0.07407 + 0.48274z \tag{2}$$

The angle between the focal plane and the z-axis is then 25.77°. The maximum distance between the fitted line and the the actual focal plane is 1.8 mm. This would seem to be sufficiently close if we were to use this focal plane location to put the first wire chamber layer.

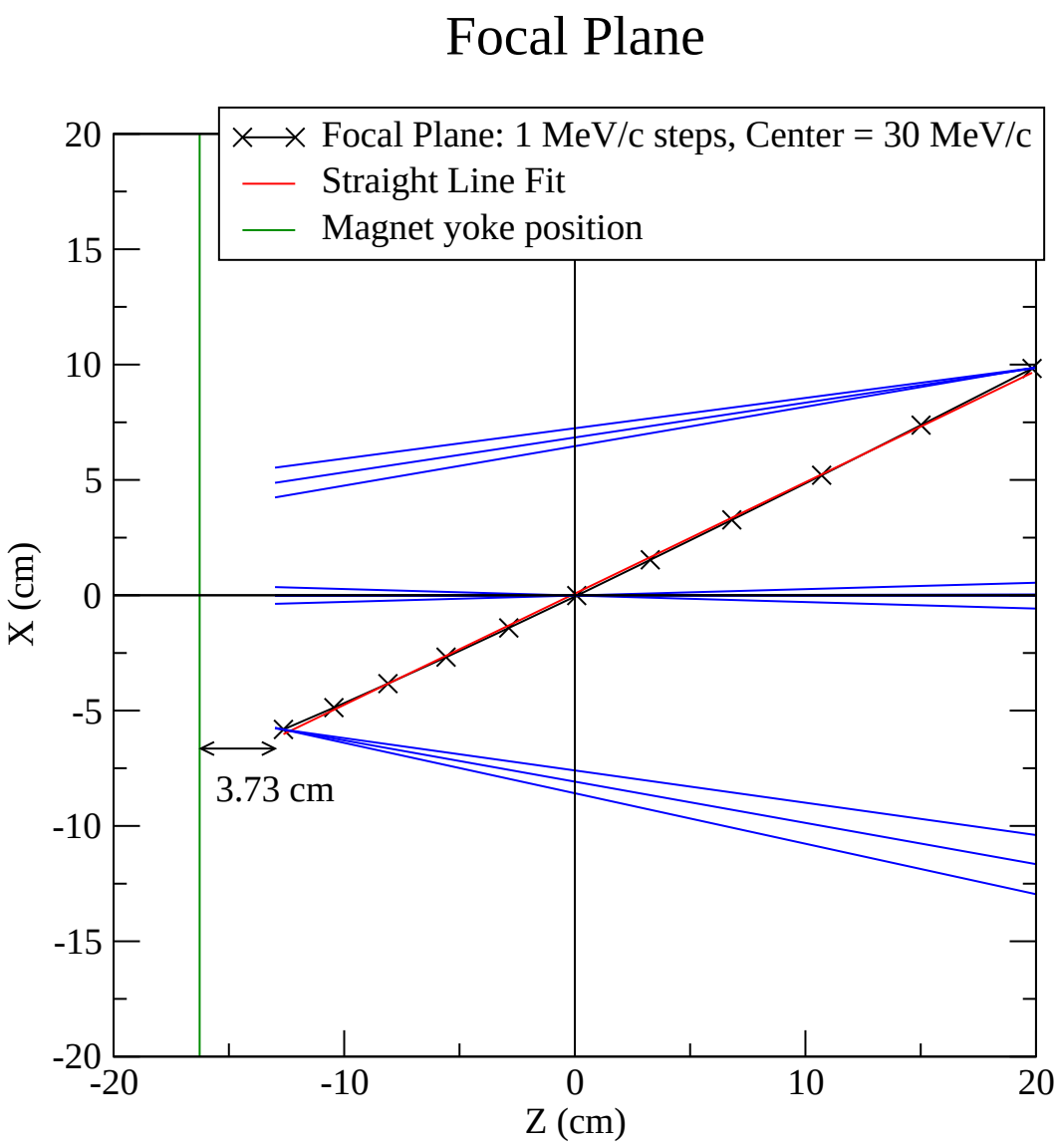

Figure 3: The focal plane of the magnet in a coordinate system centered on the focal point for a 30 MeV/c electron. Focal points are shown in 1 MeV/c steps from 25 MeV/c to 35 MeV/c. The blue lines show rays for 25 MeV/c, 30 MeV/c, and 35 MeV/c where the electron angle from the target is 0 and ± 30 mr. Note that there is only 3.73 cm between the low momentum end of the focal plane and the magnet yoke.

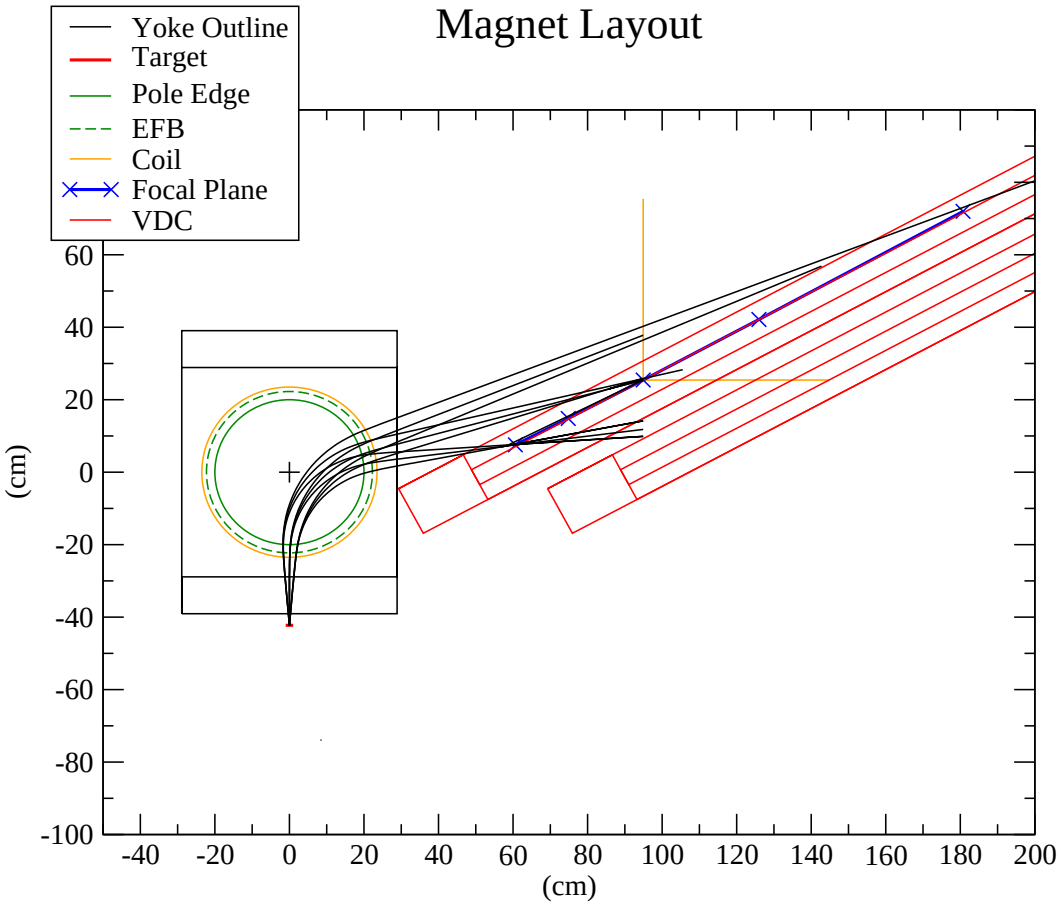

Figure 4: A possible magnet layout that uses the VDC aligned along magnet focal plane. The second VDC has been arbitrarily placed a horizontal distance of 40 cm behind the first for illustrative purposes. The rays drawn range from 26 MeV/c to 34 MeV/c.

However, the proximity of the low energy end of the focal plane to the magnet yoke would preclude the use of the Vertical Drift Chamber (VDC) to make use of the full focal plane. Such a configuration is illustrated in Figure 4. As well, the extreme angle of the focal plane would mean that the VDC, in its current configuration, would not be able to use a significant fraction of the energy acceptance. The VDC is currently set up to be used with most of the rays at about 45° to the VDC plane. There is concern that the more extreme angles of most electron tracks through the VDC will negatively affect the angular resolution of the system due to multiple scattering. As well, the current support structure for the VDCs could not be used in this configuration. Therefore the possibility of not using the focal plane is considered below (section 5).

4 Angular Acceptance

We first consider the overall angular acceptance of electron/positron tracks from the target.

The vertical angles that can make it through the spectrometer is limited by the pole gap of the magnet (2 inches = 5.08 cm). The average path length from the target to the exit magnet edge is about 58 cm. Therefore the largest vertical angle that can be accepted is $\pm 2.5^\circ = \pm 44$ mr.

The horizontal acceptance is limited by the hole in the yoke through which the electron pass from the target. The diameter of this hole is 7 cm. Therefore, with the target 3.2 cm from the pole edge, and with the thickness of the yoke being 4 inches, the maximum horizontal angle for rays starting from the center of the target is $\pm 14.7^\circ = \pm 256$ mr.

A discussion of the physics suggests that the largest asymmetries occur at the largest opening angles. Therefore we will try to optimize the magnet layout to give acceptable resolution for targets opening angles that can be accepted by the spectrometer. Later we will investigate the possibility of increasing the opening angle acceptance by moving the target position closer to the magnet yoke. However, in the initial design stages we limit the opening angles to the above extremes.

Using these extremes, rays of various energies have been traced through the magnet. The results are illustrated in figure 5. It can be seen that an energy range from 24 MeV to 42 MeV can be traced through the magnet. A much wider range is likely possible if necessary. This will depend on the energy resolution obtainable, and on how much of the VDCs can be instrumented.

5 A Software Spectrometer

Since it is not possible to use the VDCs on the focal plane we investigate the possibility of using the magnet as a software spectrometer. That is, relying on the position and angle resolution of the VDCs to allow the electron or positron parameters at the target position to be reconstructed. A possible location and orientation of the VDC is shown in figure 5. A side view is shown in figure 6. In these figures the VDC has been placed so that it is a reasonably safe distance from the magnet yoke and orientated at an angle of 90° to the central energy ray that emerges from the magnet at right angles. The center of the first VDC is at 75.0 cm from the center of the magnet. The two VDCs are shown in their current configuration using the existing 'Z'-plate mount and with the dispersive plane along the long axis of the VDCs. The two VDC are at 45° to the incident central energy ray. This is the orientation that allows the best position resolution from the VDCs.

We initially use RAYTRACE to see if this configuration can provide sufficient energy and angle resolution based on the optics alone (i.e. ignoring realistic effects such as multiple scattering).

RAYTRACE allows us to send electrons from any position on the target, with any angle and energy. We use RAYTRACE to find the final location of the ray when it intersects the plane of the first VDC. The angle of this ray can also be determined. We use the following coordinate systems to specify the initial and final particle coordinates.

The initial coordinate system is centered on the target with the $+z$ direction towards the center of the magnet and $+y$ up. As shown in figure 7 the angles θ and ϕ of a particle's trajectory are the angles relative to the $+z$ direction in the $x - z$ plane and the $y - z$

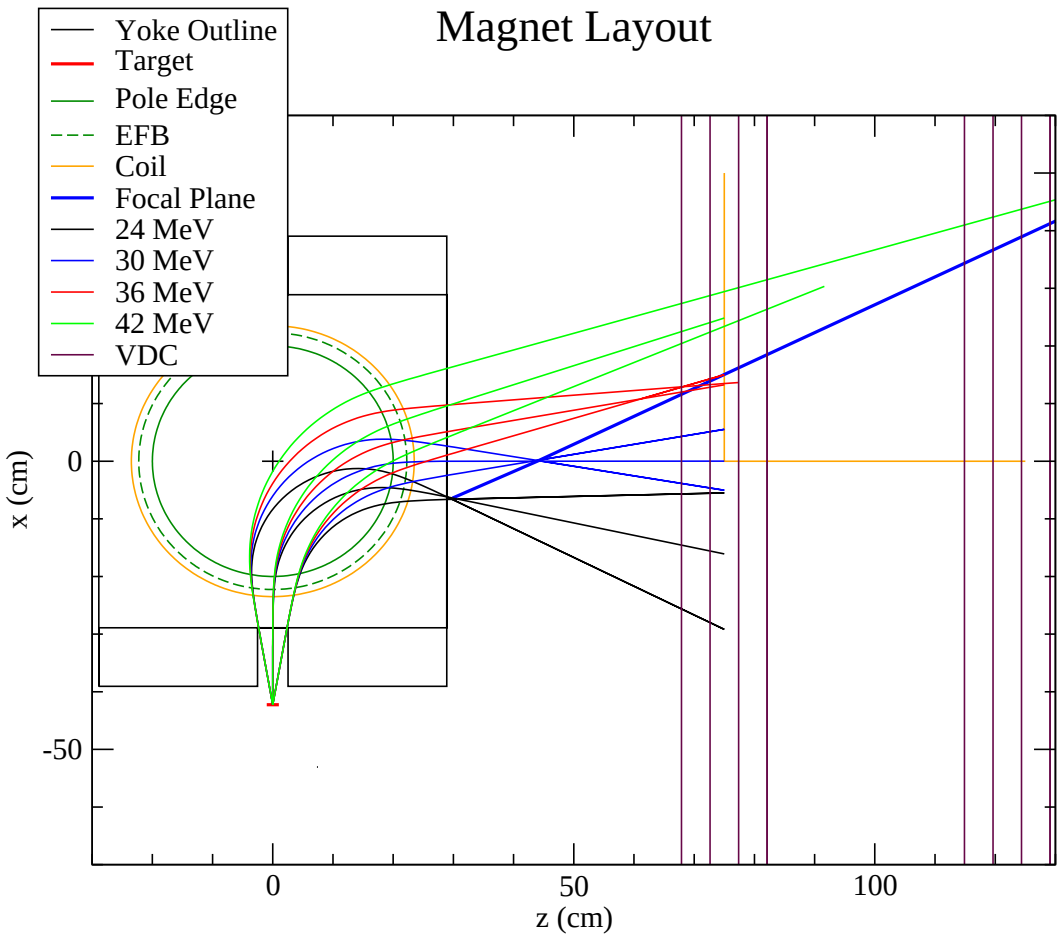

Figure 5: An illustration of the energy range that can be accepted through the magnet. Each energy is traced from the center of the target with a horizontal angular range of $\pm 10°$. The focal plane is only drawn connecting the foci at 24, 30, 36, and 42 MeV. The magnetic field has been adjusted so that 30 MeV emerges at close to a right angle with respect to the incident beam direction. The maroon lines show a possible location of the VDCs.

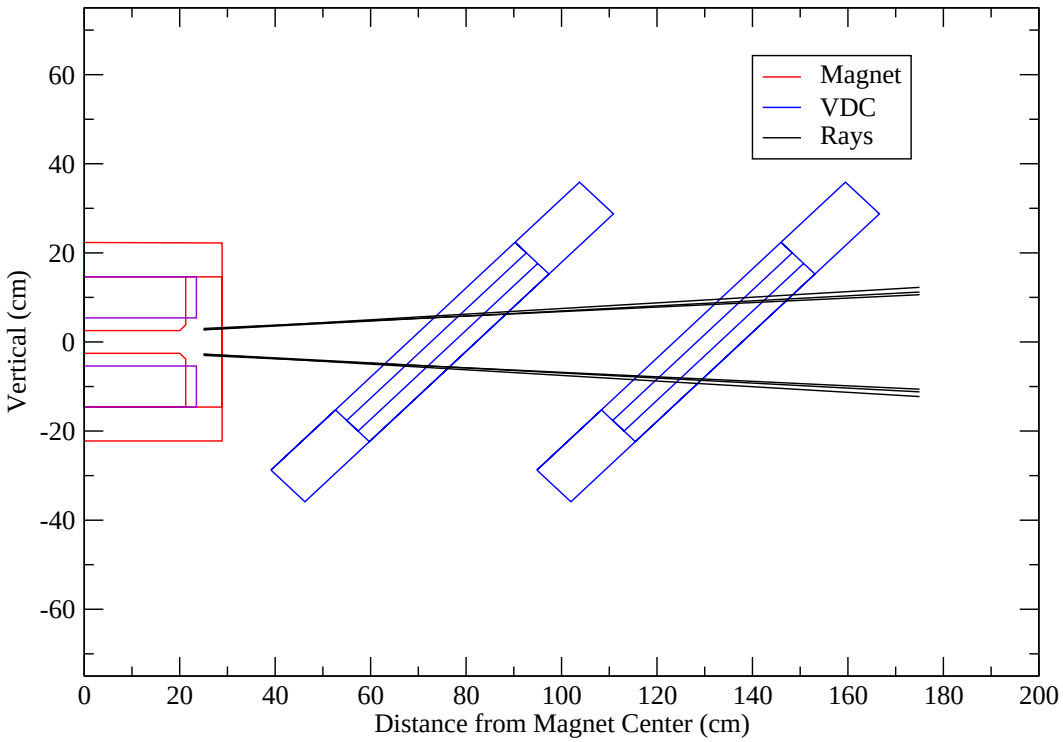

Figure 6: A side view of the magnet and a possible location for the VDCs. The rays shown are those for the most extreme vertical angles that can pass through the magnet, and for the energy range between 24 and 42 MeV.

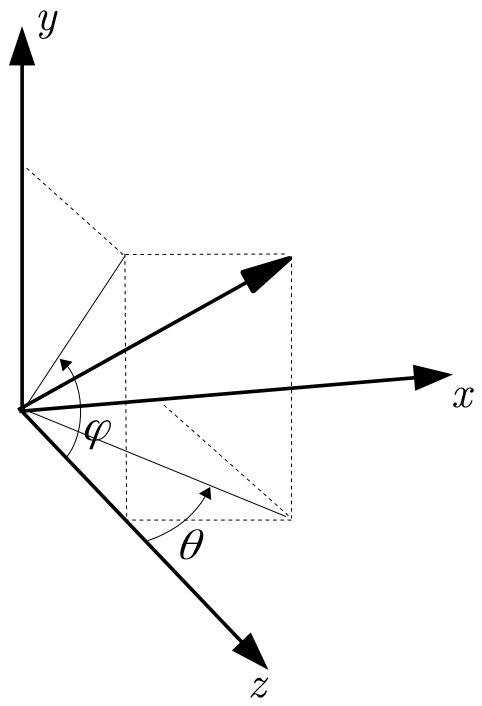

Figure 7: The definitions of the coordinate system used by RAYTRACE to specify the particle trajectory.

plane respectively. This coordinate system follows the way RAYTRACE defines the particle momentum directions.

The initial coordinates of a particle at the target is given by x_i and y_i and its angle specified by θ_i and ϕ_i. The energy of the initial particle is specified relative to a central energy E_0 by the quantity δ. δ is given as a percentage defined by $\delta = (E - E_0)/E_0\%$ for a particle of energy E. In our case we have defined $E_0 = 30$ MeV.

At the first VDC we record the position of the particle by x_f and y_f where the $x-y$ plane is in the plane of the VDC. x_f is along the long axis of the VDC (parallel to the beam axis), y_f is along the short axis of the VDC, and z_f is perpendicular to the VDC. The locations of the track through the second VDC is used to determine the angle θ_f and ϕ_f of the track relative to the coordinate system at the first VDC.

Our problem is to determine δ, θ_i and ϕ_i from the measured x_f, y_f, θ_f and ϕ_f. From RAYTRACE we find that the quantities y_f and ϕ_f are strongly correlated and, to first order, depend only on ϕ_i. This leaves the two quantities x_f and θ_f from which we need to determine δ and θ_i. Unfortunately the system is under-determined since the measured quantities x_f and θ_f also depend on the the particle's initial position on the target x_i (and y_i). x_i and y_i are not known exactly since there is a finite size photon beam spot on the target. We must therefore take the approach of determining a best fit between the measured quantities x_f, y_f, θ_f and ϕ_f and the required quantities δ, θ_i and ϕ_i.

We first used the facility of RAYTRACE to calculate the first order transfer matrix

elements from input to final quantities assuming that the rays all start from $x_i = 0$ and $y_i = 0$. From this we can calculate a first order estimate of the expected resolutions given that we will have a finite beam size and there is finite position resolutions at the VDCs. This showed that, at least in this simple approximation, reasonable resolutions would be possible. However this does not take into account the higher order terms in the transfer function.

Next we used a Monte-Carlo approach. We initially ran a large number of individual rays through RAYTRACE with random initial values for δ, θ_i and ϕ_i within the expected ranges, but with $x_i = 0$ and $y_i = 0$. We smeared the output quantities with the expected resolution of the VDC. We then fitted these rays to determine functions to calculate δ and θ_i from the final quantities. The we ran a second set of rays through RAYTRACE, but this time allowing x_i and y_i to be within the expected beam spot. We calculated the difference between the reconstructed δ and θ_i, calculated using the functions we found from the first run, and the actual input values of δ and θ_i. Such comparisons showed that we should be able to achieve energy resolutions of the order 2 MeV and angular resolutions of the order less than 2°. However these tests, while encouraging, do not take into account the realities of the geometry and the effects of multiple scattering. A full simulation of the magnet system is needed.

6 GEANT4 Simulation

A summer student, David Fairbairn, worked on incorporating the measured magnetic field map into GEANT4. Subsequently, graduate student, Glen Pridham, took David's work and included it into a simulation that included the magnet hardware, pole pieces, yoke and coil. For rays that stayed within the magnet central plane, Glen was able to show that GEANT4 reproduced the predictions of RAYTRACE under those ideal conditions. This simulation was used as the basis for further development.

A serious limitation of the simulation was that the magnetic field was assumed to be uniform in the vertical direction. That is the field is assumed to be the same as it is in the horizontal median plane (which is where we have our only field measurements).

I therefore modified the code so that, instead of using a look-up table for the magnetic field, and interpolating to find the field at any point, a parameterization of the field was used. In fact the same algorithm that is used by RAYTRACE was employed to calculate the magnetic field and direction at any point in space. This then would correctly simulate the effects of the fringe field near the pole edges. Checks we done to ensure that the magnetic field calculated by the GEANT4 simulation were the same as those calculated by RAYTRACE at each point in space.

In the simulation, as originally put together by Glen, the VDCs were implemented assuming that we would only record a hit at the nearest wire in each VDC layer. In other words the position resolution of the VDCs would be the wire spacing. This would have allowed for much simplified instrumentation. However, subsequent calculations and tests using the simulation showed that we would not be able to achieve the required angular resolution when using the VDCs in this mode.

The profile of the VDC, as subsequently implemented in the simulation, is shown in

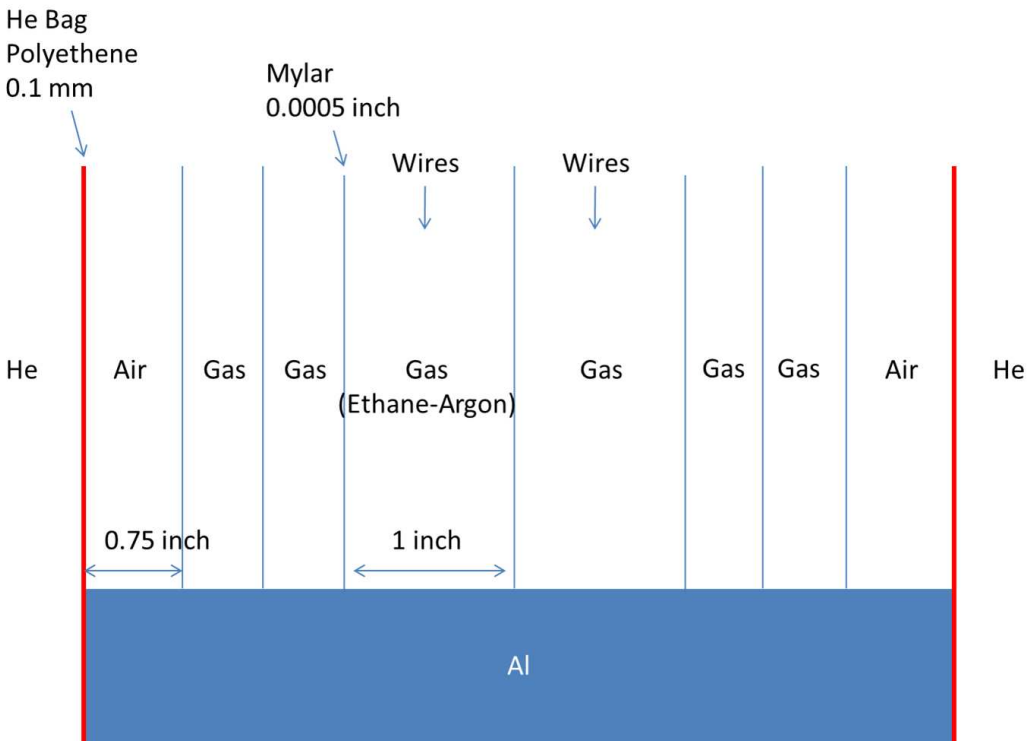

Figure 8: Profile of the VDC as implemented in GEANT4.

figure 8. The wires themselves are not included in the simulation. The gas layers where the wires are, are made to be "sensitive" in the simulation. Whenever energy is deposited in that sensitive area the position and energy deposited is recorded. The hit position in that gas layer is calculated by averaging the positions, weighted by the energy deposited. A minimum total energy must be deposited in each gas layer before there is considered to be a hit on that VDC. At present that minimum is set to 0.2 keV. The hit position on the VDC is then calculated by averaging the hit positions in the two gas layers. Finally the hit position is smeared, in both the x and y directions, by adding a random number chosen from a Gaussian with a standard deviation of 0.1 mm. This is consistent with the VDC resolution reported in the thesis by Leckey [5].

A picture showing the GEANT4 rendering of an early versions of the simulation is shown in figure 9. Note that the VDC are now located with their long axis parallel to the beam direction. The existing mounting system for the VDC pair is employed and the VDCs are at 45° to the vertical with the top furthest from the magnet. Subsequently the VDCs were realigned so that the tops are closest to the magnet. This was to allow more room for a support structure beneath the VDCs. Changing this orientation does not affect the resolution of the system.

he background material, through which the electrons or positrons travel, is helium gas at atmospheric pressure. Therefore in the simulation there is included a 0.1 mm thick polyethylene bag to contain this helium. There is a bag layer just after the target, which is

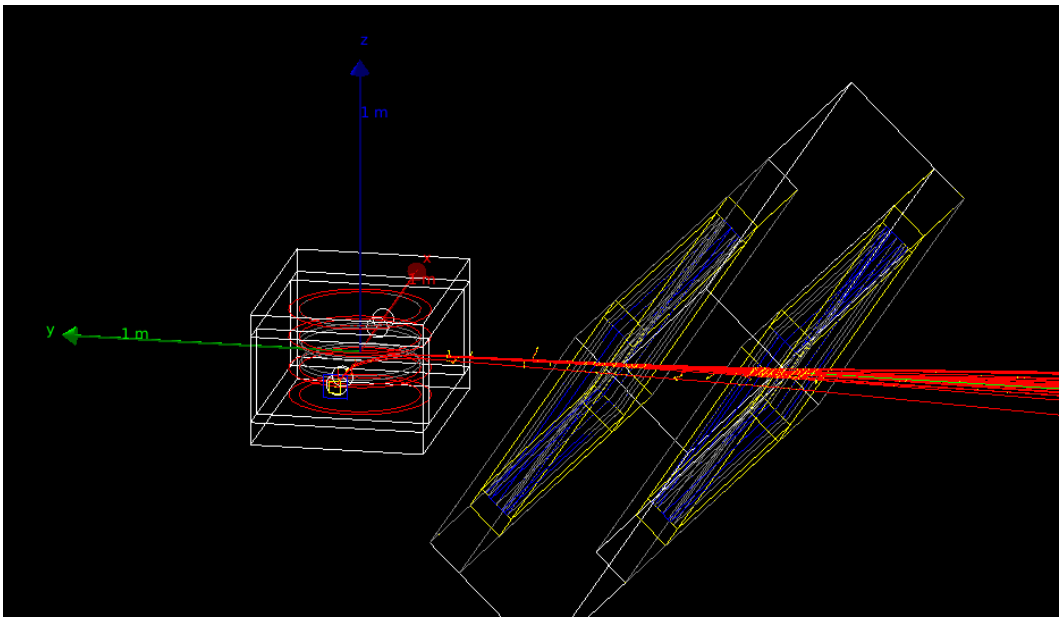

Figure 9: An early version of the magnet and VDC locations as rendered by GEANT4.

in air, and we have included a bag interface at the front and back of each VDC, as can be seen in figure 8. (Later we investigate the possibility of not using a helium bag at all.)

With this version of the simulation we investigated the energy and angular resolutions we can obtain. We use the same procedure as we did for the investigation using RAYTRACE. We use electrons generated within the target with parameters selected at random. First we choose a source position for an electron at a random depth within the thickness of the target. We choose a random δ_i between -20% and $+40\%$. The central energy is 30 MeV. The magnetic field at the center of the magnet is set to -0.4536 Tesla. At this field a 30 MeV electron emerges from the magnet at nearly 90° from the beam direction, if $\theta_i = 0$. We choose random values of θ_i and ϕ_i between the ranges described in section 4 For each track we record the position on each VDC. From the positions on the two VDCs we calculate the angles of the track at the first VDC (θ_f and ϕ_f). The final position (x_f and y_f) is the position at the first VDC. The definition of this coordinate system is detailed in the following paragraph. (For convenience this is chosen to be the same coordinate system as used by RAYTRACE.)

The origin of the coordinate system is at the center of the first VDC in each VDC pair. The z direction is perpendicular to the VDC and pointing away from the magnetic spectrometer. The x direction is along the long axis of the VDC and parallel to photon beam direction. For the VDC package on beam right $+x$ is in the same direction as the beam direction. For the VDC package on beam left $+x$ is in the opposite direction to the beam direction. The y direction is up and parallel to the face of the VDC. Because of the 45° tilt of the VDC, the z and y axes are of course at 45° to the horizontal and vertical directions. As shown in figure 7 the angles θ and ϕ of a particle's trajectory are the angles relative to the $+z$ direction in the $x - z$ plane and the $y - z$ plane respectively.

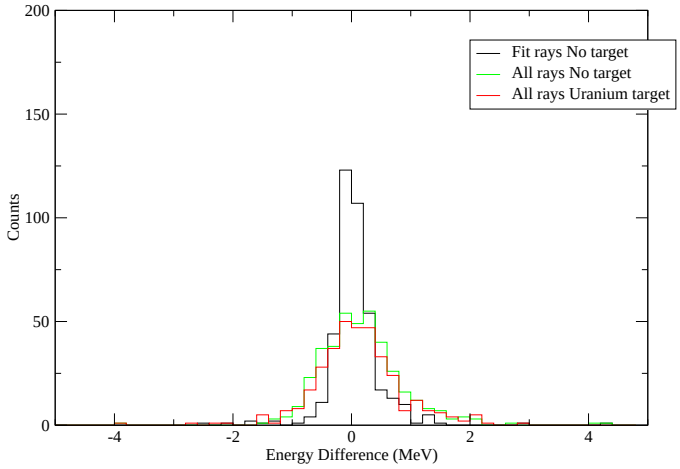

Figure 10: An early version of the GEANT4 prediction for $E_i^{fit} - E_i^{input}$ for three simulation as described in the text.

For a set of tracks where the source position has no size (i.e. $x_i = y_i = 0$) we find functions that are a best fit to

$$\delta_i = f_\delta(x_f, \theta_f) \qquad \text{and} \qquad \theta_i = f_\theta(x_f, \theta_f)$$

The form of the functions were simple polynomials at this stage. Figures 10 and 11 show histograms of $E_i^{fit} - E_i^{input}$ and $\theta_i^{fit} - \theta_i^{input}$ respectively for three different simulation data sets. The first set is the set used for the fitting, where there was no actual target (the target material was replace with vacuum) and the source position has no size. The second set is also with no target, but the source position has x_i and y_i chosen randomly within a realistic beam spot size (1/2 inch diameter). The third set is with a realistic beam spot size and with the target replace with uranium (with thickness 0.025 mm). The effects of the finite beam spot and the multiple scattering in the target are clear in the energy difference plot, but the difference are not so apparent in the angle difference plot. Apparently the angular resolution is more influenced by the resolution of the VDCs.

Note that for the θ difference distribution in figure 11 the width is the distribution does not change much when the uranium target is added, but the height of the distribution decreases. This is apparently because the multiple scattering in the target causes some some electrons to never reach the VDCs. But for those electrons that do, the tracking back to the target is not affected much.

Several variations of the absolute location of the VDC were tried. It was found that the ultimate resolutions depended very weakly on the actual locations of the VDC. Therefore locations convenient for the support structure were chosen for further study.

At this point additions to the simulation were made to include a second VDC package on beam left. As well a plastic scintillator hodoscope package was included behind each VDC package. In the simulation a hit on the hodoscope is required before "readout" of the VDC occurs as will be required in the actual experiment. This places limits on the energy range, and to some extent the angular range accepted by the spectrometer.

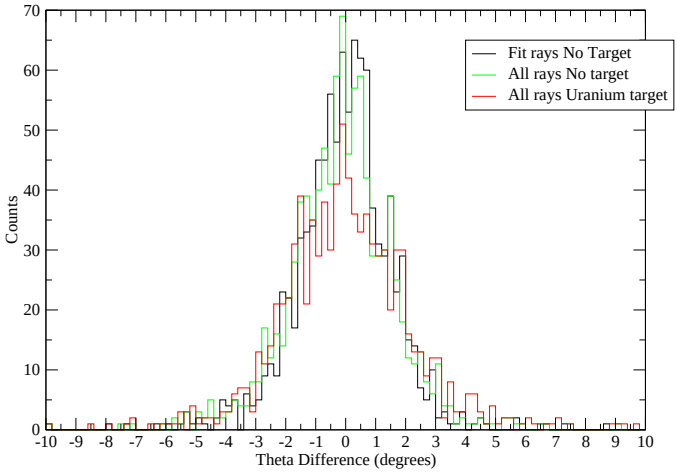

Figure 11: An early version of the GEANT4 prediction for $\theta_i^{fit} - \theta_i^{input}$ for three simulation as described in the text.

The next section sets out the locations of some critical items we have agreed on.

7 Spectrometer Layout Dimensions

Critical layout dimensions are given in table 1. The coordinate system for locating items is the same as used in figure 5 with the origin at the magnet center. The center of the hodoscope is defined at the depth between the front and back paddles.

The external dimensions for the VDCs are 96 inch, 243.84 cm, long with a thickness of 5.5 inch, 13.97 cm. The active parts of the VDCs start 19.7 cm from the ends. From Table 1 it can be seen that a length of approximately $32.6 + 34.2 = 66.8$ cm of VDC-1 must be instrumented. For VDC-2 a length of approximately $45.8 + 58.2 = 104.0$ cm must be instrumented.

A GEANT4 rendering of the magnet, VDCs and hodoscope with these layout parameters is shown in figure 12.

Table 1: Locations of critical items.

Item	z (cm)	x (cm)	y (cm)
Center of magnet pole	0	0	0
Right magnet yoke corners	+28.90	−39.05	−22.23
	+28.90	−39.05	+22.23
	+28.90	+39.05	+22.23
	+28.90	+39.05	−22.23
Target center	0	−42.26	0
Center of VDC-1	+85.00	0.00	0
Extreme rays on VDC-1	+85.00	−34.2	0
	+85.00	+32.6	0
Center of VDC-2	+132.00	0.00	0
Extreme rays on VDC-2	+132.00	−58.2	0
	+132.00	+45.8	0
Center of Hodoscope	+185.00	0	0

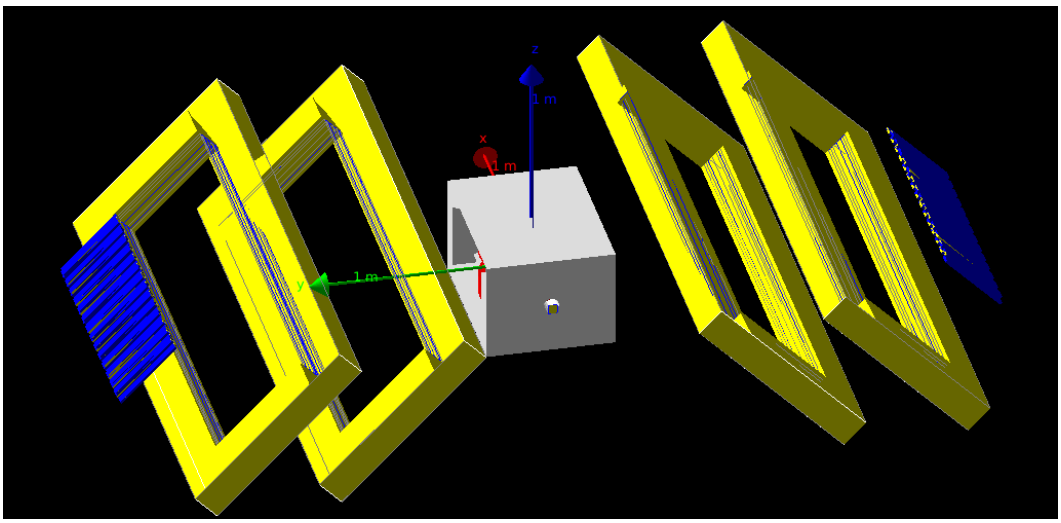

Figure 12: GEANT4 rendering of pair spectrometer magnet with the VDC and hodoscope packages.

8 Spectrometer Performance

Using the parameters obtained for the configuration defined in the previous section, one can construct histograms to determine the resolution obtainable for both electrons and positrons. Plotted in each of the histograms in figures 13, 14, 15 and 16 is the difference between the input quantity and the reconstructed quantity for various data sets. Data set 1, shown in black, is when all event start at $x_i = y_i = 0$ on the target, but with the target replace with a vacuum. Data set 2, shown in red, is when all events are distributed over a 1/2 inch beam spot on the target, but with the target replace with a vacuum. Data set 3, shown in green, is when all events are distributed over a 1/2 inch beam spot on the target, and the target is the 0.025 mm thick Uranium target. The polar angle is the angle between the beam direction and the angle of the particle emerging from the target.

As can be seen from these histograms we come to the same conclusion as we did from the earlier version of the simulation. Namely, that the resolution, for those events that reach the detectors, does not degrade appreciably due to the finite beam spot size. Also the resolution is reduced by the multiple scattering in the target, but only by a small amount. We do lose some more events but these are particles that do not reach the detector and therefore will not be seen in the experiment.

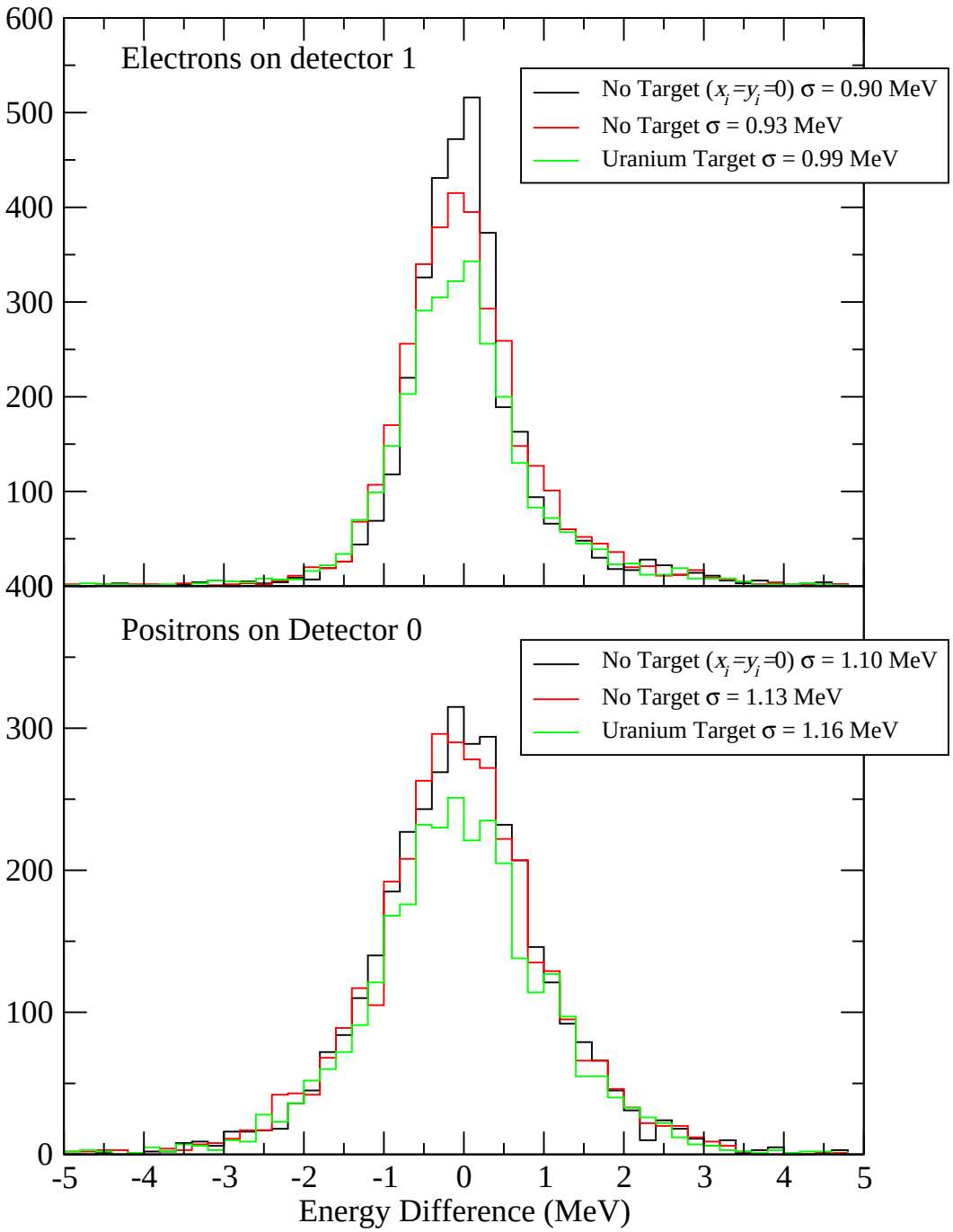

Figure 13: Difference between reconstructed and input energy E_i at target.

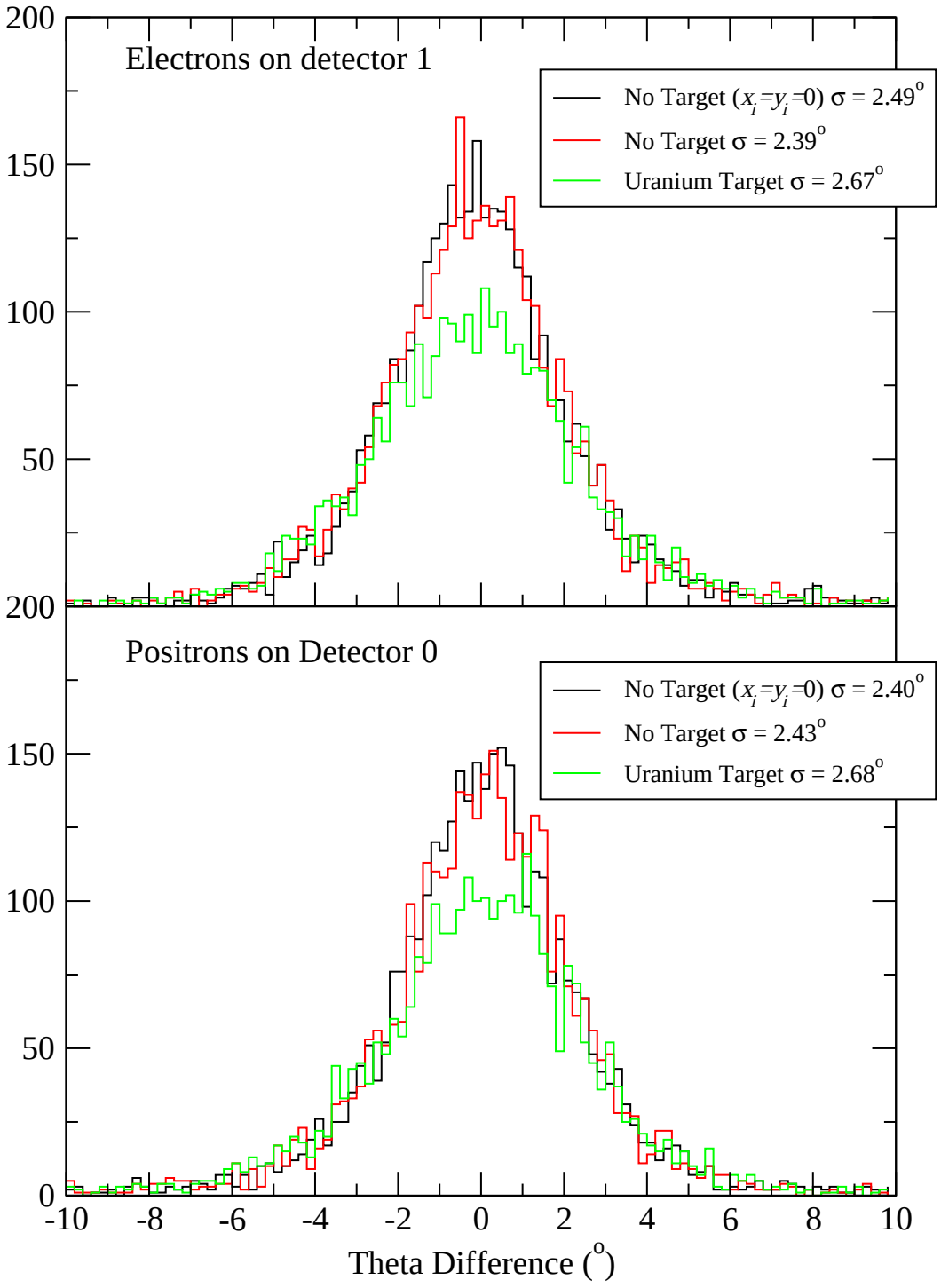

Figure 14: Difference between reconstructed and input angle θ_i at target.

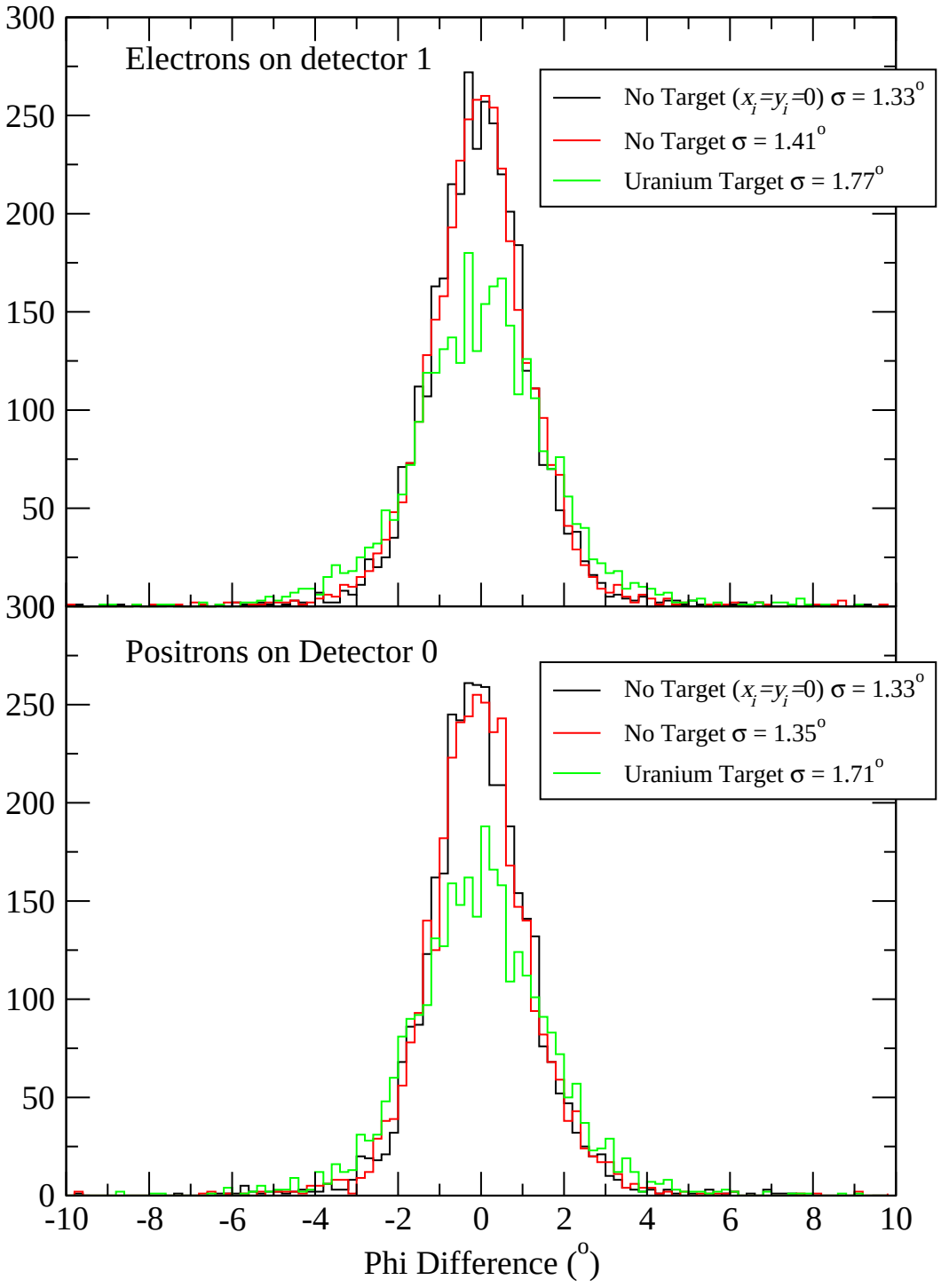

Figure 15: Difference between reconstructed and input angle ϕ_i at target.

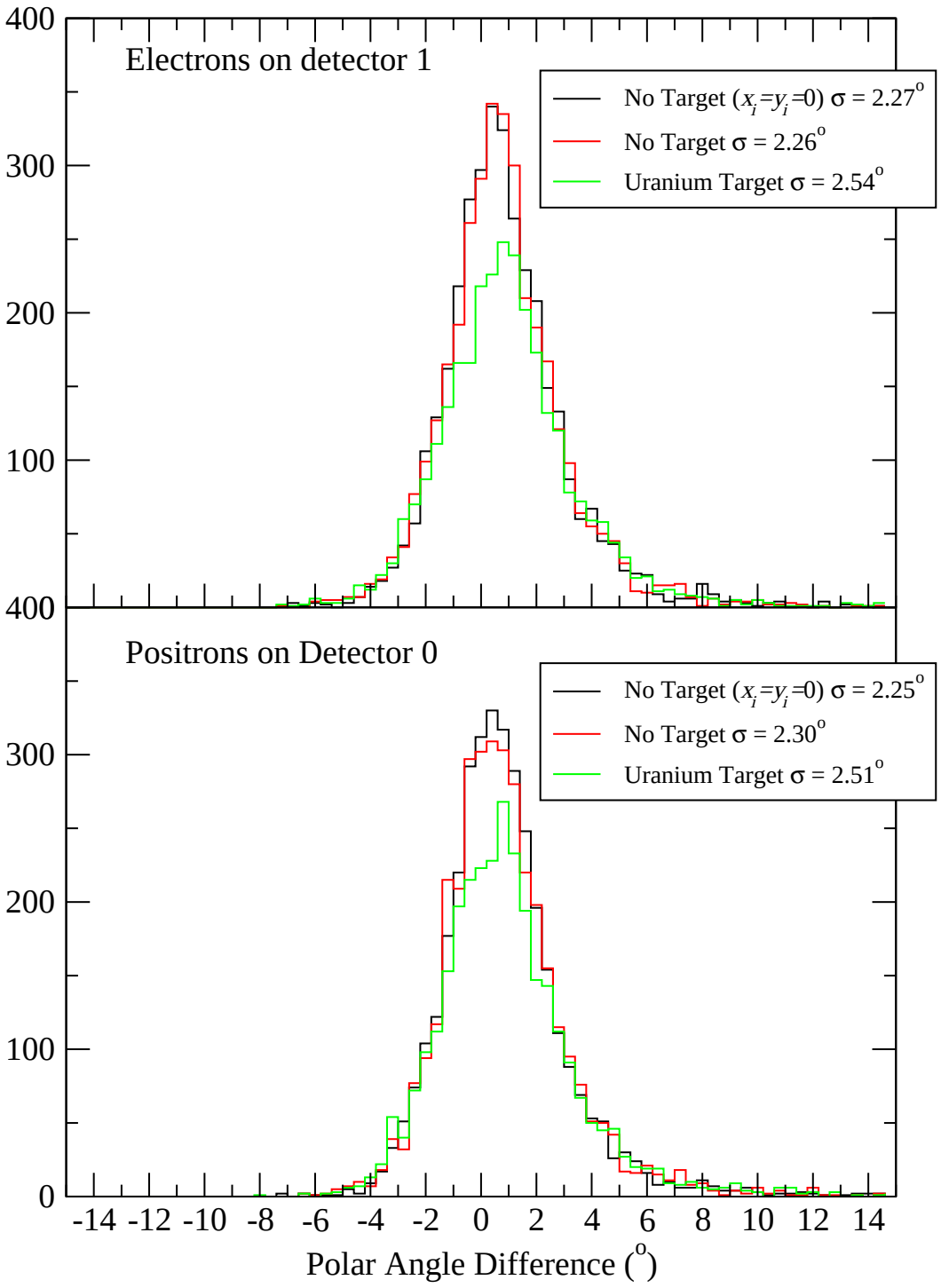

Figure 16: Difference between reconstructed and input polar angle at target.

9 Asymmetry Tests

To allow consistency checks, a new feature was added to the simulation. An invisible sensitive "detector" was added just after the target. This sensitive volume just records the energy and angles of electrons and positrons passing through it. I have called this the "monitor". One purpose of the monitor is to confirm that the simulation is producing particles correctly. For example the histograms in figure 17 show the difference between the polar angle generated within the target and the polar angle recorded in the monitor. As expected there is no difference when the target is a vacuum, but the multiple scattering within the uranium target is clearly seen.

A second use of the monitor is to check in the asymmetry of events produced within the target so that it might be compared to the asymmetry we can measure after reconstruction of the tracks.

Another feature of the simulation is the ability of generating photons upstream of the target and allowing the electromagnetic interactions included in the GEANT4 package to produce electron/positron pairs within the target. It is expected that the pair production calculation used in GEANT4 will not include the higher order terms that contribute to the asymmetry we are trying to measure in this experiment. Nevertheless it is instructive to see how the reconstruction using the spectrometer reproduces the asymmetry generated by GEANT4.

The asymmetry for a given polar angle is defined by

$$\epsilon(\delta) = \frac{N_+ - N_-}{N_+ + N_-} \tag{3}$$

Here there is a requirement that the electron and positron be in the same plane which is also in the same plane as the incident photon, and that the polar angle of the electron is the same as the polar angle of the positron. δ in this context is the energy difference between the electron and positron, i.e. $\delta = E(e^-) - E(e^+)$. Then N_+ is the number of events that have met the angle condition and δ is positive while N_- is when δ is negative. The definition of the asymmetry forces it to have negative symmetry about $\delta = 0$, i.e. $\epsilon(-\delta) = -\epsilon(\delta)$.

We can calculate this asymmetry for the electrons and positron measured by the monitor and we can calculate it for the asymmetry using the energies and angles reconstructed from the detector. The stringency of the condition on the angular symmetry was chosen to be consistent with the resolutions we observe. The result is shown in figure 18. As expected, the asymmetry generated by GEANT4 is essentially zero, and, within uncertainties, the asymmetry reconstructed from the spectrometer is also zero.

There are a number of uncertainties associated with this test. First the number of events run in the simulation was limited and therefore the the uncertainties are large. Second and more importantly, the quality of the fitting function had not yet been fully verified. It took a long time to find the parameters of that fitting function and it was desired to find a better process for finding these parameters so that a new set of fitting functions could be found quickly when changes to the spectrometer and detector lay were changed. There were a number of variations in the setup, e.g. target position and VDC location, that we wished to investigate. It was important then to be able to compare results from setup changes, with

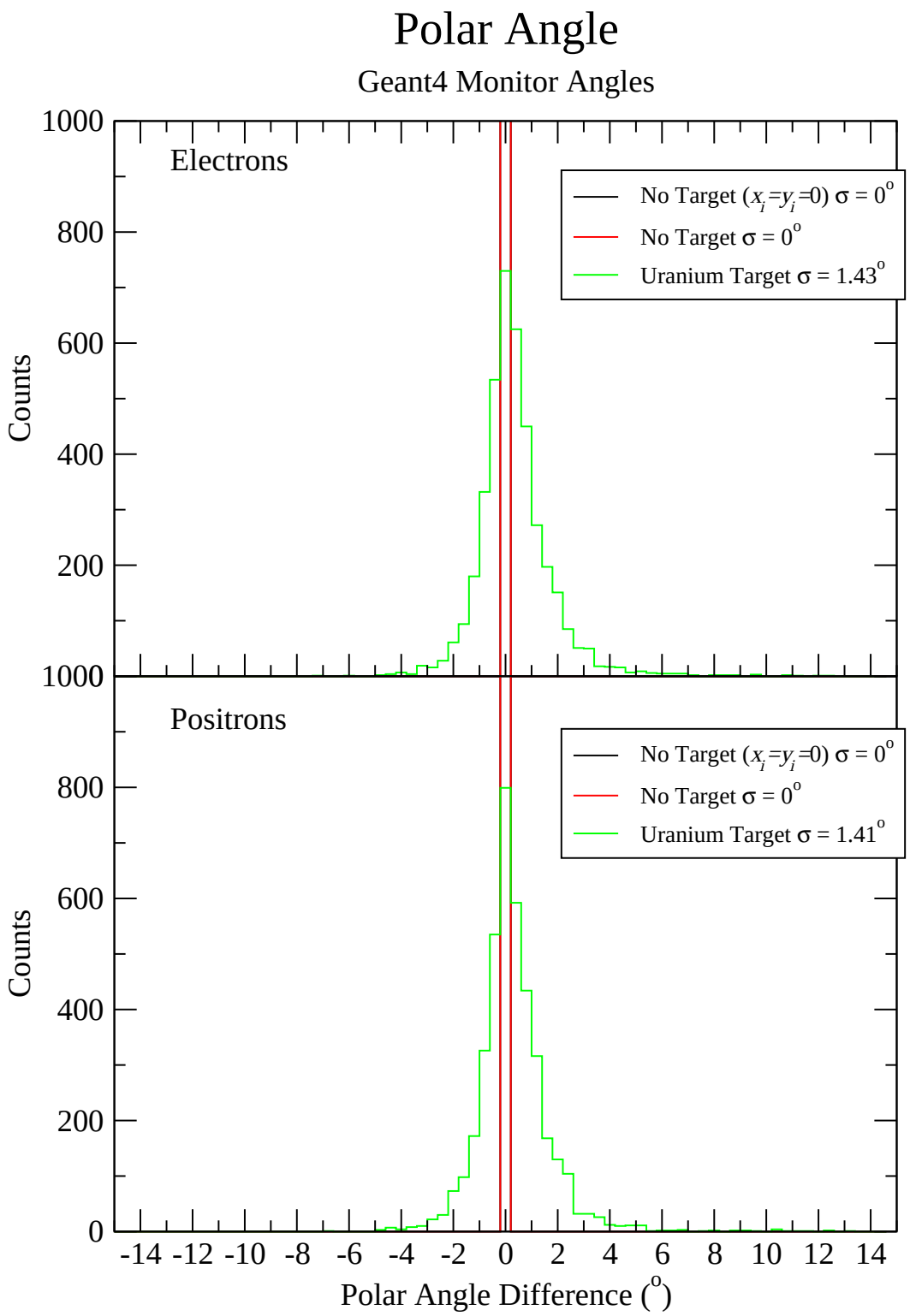

Figure 17: Difference between the input polar angle generated with the target and the polar angle as measured in the "monitor" just after the target.

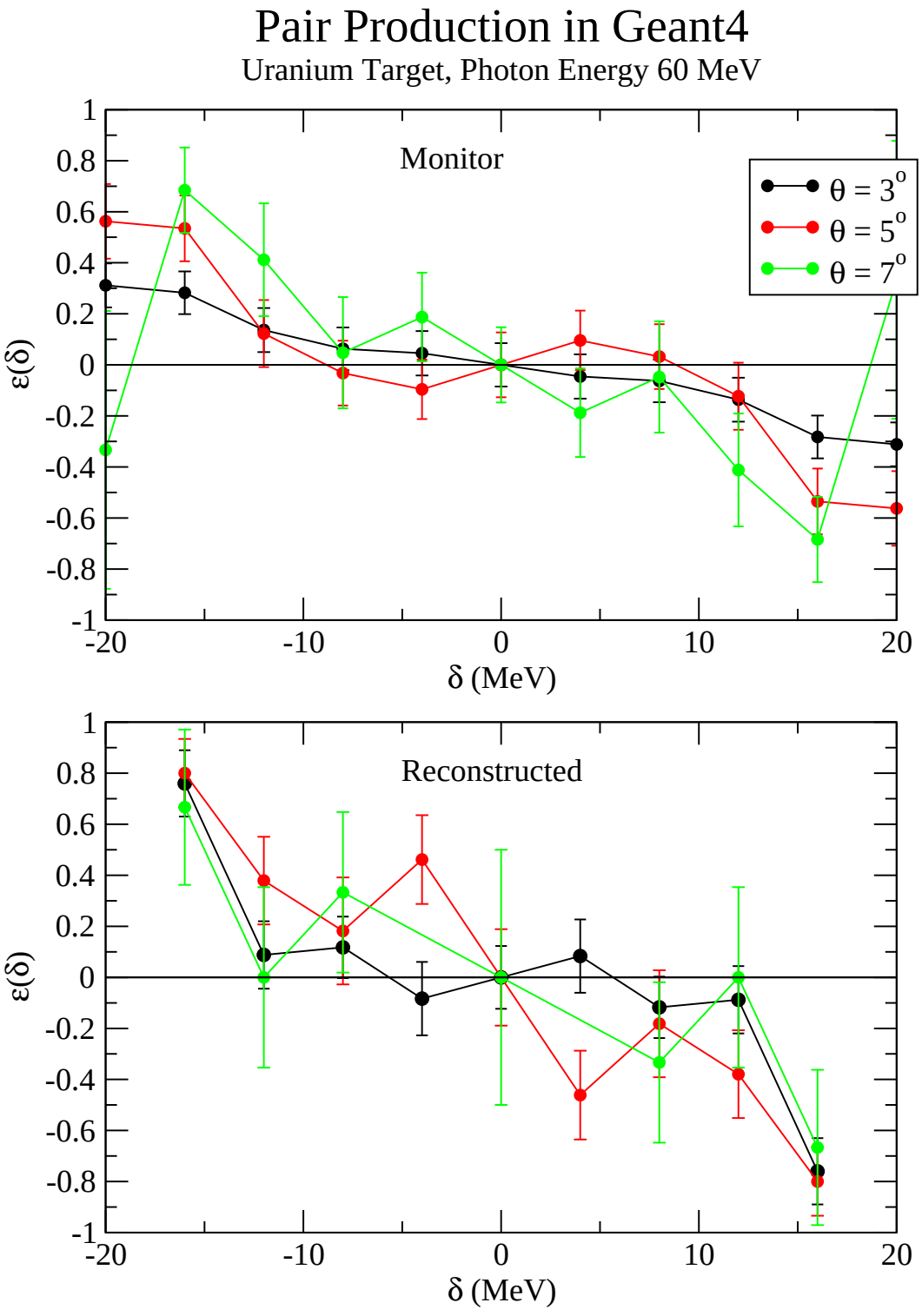

Figure 18: The asymmetry as calculated from the monitor and from the reconstructed tracks.

the worry that any change we observe in resolution, were in fact due to the change in setup, and not just due to the fact that we may have not yet found an optimum fitting function for the new setup.

Up to this point the analysis of the simulation output had been accomplished with a set of Perl scripts, which, while serving the purpose, did not allow quick changes to be made, and perhaps restricted the level of analysis that could be accomplished with a system such as root.

10 Reconstruction Parameter Fitting

With the spectrometer layout approximately defined a refinement of the method for reconstructing the energy and angles at the target was undertaken. A set of root codes were written to take the output of the GEANT4 simulation and find the fitting parameters. The generalized fitting functions used are given by equations (4), (5) and (6).

$$\delta_i^{fit} = a_0(x_f) + a_1(x_f)\theta_f + a_2(x_f){\theta_f}^2 + a_3(x_f){\theta_f}^3 \tag{4}$$

with

$$\begin{aligned} a_0(x_f) &= a_{00} + a_{01}x_f + a_{02}{x_f}^2 + a_{03}{x_f}^3 \\ a_1(x_f) &= a_{10} + a_{11}x_f + a_{12}{x_f}^2 + a_{13}{x_f}^3 \\ a_2(x_f) &= a_{20} + a_{21}x_f + a_{22}{x_f}^2 + a_{23}{x_f}^3 \\ a_3(x_f) &= a_{30} + a_{31}x_f + a_{32}{x_f}^2 + a_{33}{x_f}^3 \end{aligned}$$

$$\theta_i^{fit} = b_0(x_f) + b_1(x_f)\theta_f + b_2(x_f){\theta_f}^2 + b_3(x_f){\theta_f}^3 \tag{5}$$

with

$$\begin{aligned} b_0(x_f) &= b_{00} + b_{01}x_f + b_{02}{x_f}^2 + b_{03}{x_f}^3 \\ b_1(x_f) &= b_{10} + b_{11}x_f + b_{12}{x_f}^2 + b_{13}{x_f}^3 \\ b_2(x_f) &= b_{20} + b_{21}x_f + b_{22}{x_f}^2 + b_{23}{x_f}^3 \\ b_3(x_f) &= b_{30} + b_{31}x_f + b_{32}{x_f}^2 + b_{33}{x_f}^3 \end{aligned}$$

$$\begin{aligned} \phi_i^{fit} = c_{00} &+ c_{p1}\phi_f + c_{p2}{\phi_f}^2 + x_{p3}{\phi_f}^3 \\ &+ c_{t1}\theta_f + c_{x1}x_f \\ &+ c_{y1}y_f + c_{y2}{y_f}^2 + c_{y3}{y_f}^3 \end{aligned} \tag{6}$$

In general the higher order parameters are not needed. The fit is accomplished by running the GEANT4 simulation for a range of known input values δ_i, θ_i and ϕ_i, and minimizing a chi-squared. For example the energy parameters are found by minimizing

$$\chi^2 = \sum_{n=1}^{N} \left[\frac{\delta_{in} - {\delta_i}_n^{fit}}{{\sigma_f}_n^{fit}} \right]^2 \tag{7}$$

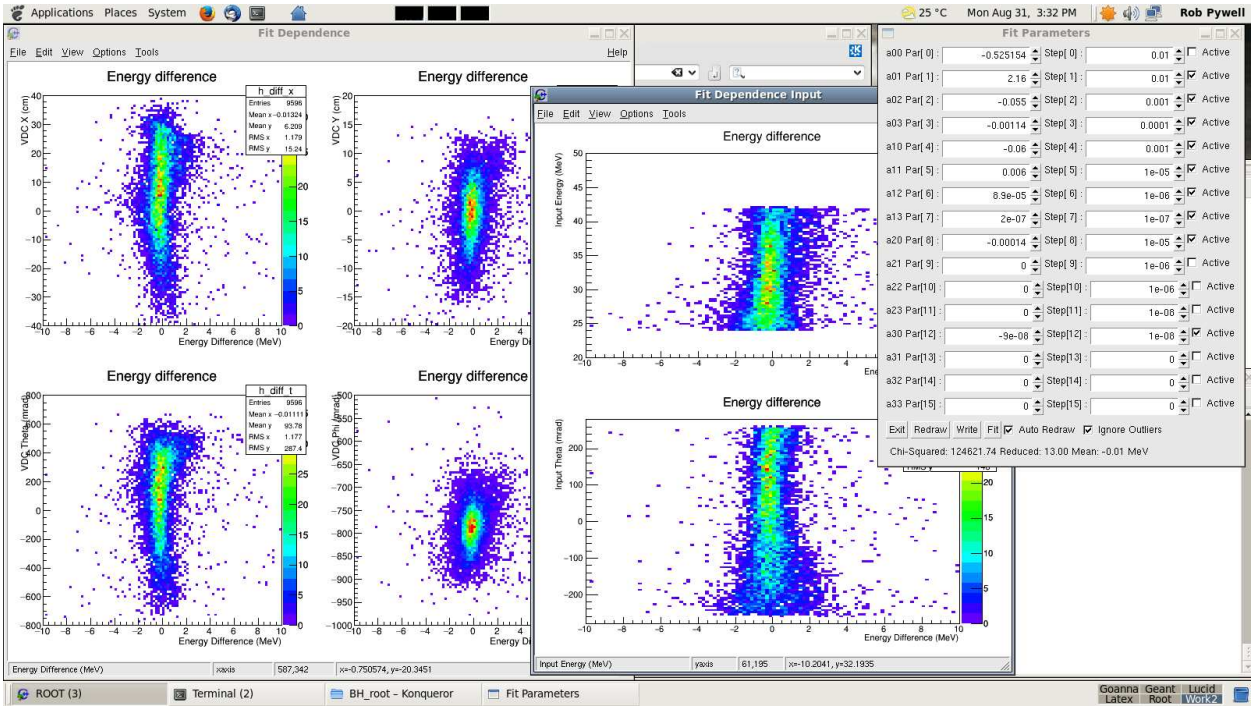

Figure 19: The root visual interface to facilitate the fitting to obtain the reconstruction algorithm for the energy.

where N is the total number of points used in the fit, and σ_f^{fit} is a standard deviation calculated using the function δ_i^{fit} and using uncertainties for x_f and θ_f. These uncertainties have been estimated from the simulation, however these are essentially fake uncertainties, and hence the actual value of the χ^2 is meaningless and cannot be used for estimating uncertainties in the fit parameters.

In general it was found that the fitting could not be done by simply using a standard minimization routine. This is assumed to be because of the potentially large number of parameters and because there appear to be a large number of local minima. The fitting process essentially had to be guided by hand to choose appropriate starting parameters and step sizes. Higher order parameters were added as the fit improved. A minimization routing was used in the final stages to improved the fit. Even after minimizing the chi-squared it was found that final adjustments needed to be made by hand. Even though a fit produced an excellent chi-squared it was sometimes found that there was an unacceptable systematic dependence on one quantity or another.

A visual interface for root has been written to facilitate this process. The quality of the fit can be displayed as a function of the various input and output quantities. A screenshot of this interface is shown in figure 19.

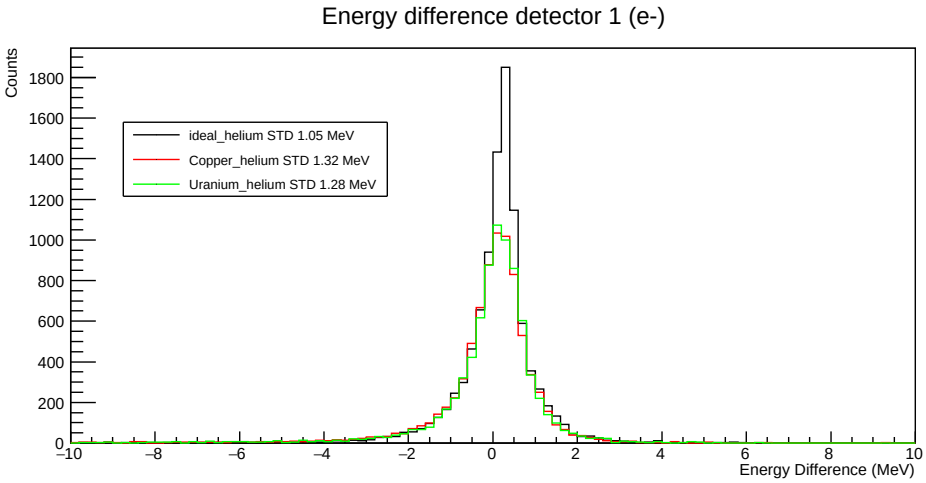

Figure 20: Comparison of the energy resolutions obtained with a 0.1 mm copper target and a 0.025 mm uranium target.

11 Targets and Count Rates

The original proposal for this experiment called for using a uranium target and possibly a carbon target. The uranium target, with thickness 0.025 mm has obtained and this has been used as a representative target in the above investigations. It was quickly realized that a carbon target would have an asymmetry that may be too small for us to measure. This is coupled with the fact that the cross section drops with smaller Z. It was decided that another target with Z much smaller than uranium, but with reasonable count rate was needed. Copper was suggested as such a target.

The simulation was used to determine maximum thickness of a copper target we could use that would preserve a reasonable resolution. The result is that a copper target with a thickness of about 0.1 mm gives about the same resolutions as we get using the 0.025 mm uranium target. This is illustrated in figures 20 and 21.

Actually it can be seen that the resolutions we get, for "good" events, are relatively weakly dependent on the target thickness. With thicker targets there are more events where the reconstructed energy or angle is extremely far off, or the particles do not even reach the detector. We will not see these in the actual experiment since we will require a coincidence between the electron in one detector and the positron in the other. i.e. This just reduces our experiment efficiency.

Reducing the efficiency is likely not a problem. With simulations using photons on the target one can get a good idea of our count rate. For a given number of photons we can measure the number of times we get a hit on both the left and right detectors. A hit is defined as a hit in the hodoscope and the VDC. We can then also calculate the rate of pairs that pass the symmetry cuts (but of course that is spread over all the angle and delta values). For a beam rate of about 3.5×10^6 /s (as in the original proposal) we get the following count rates.

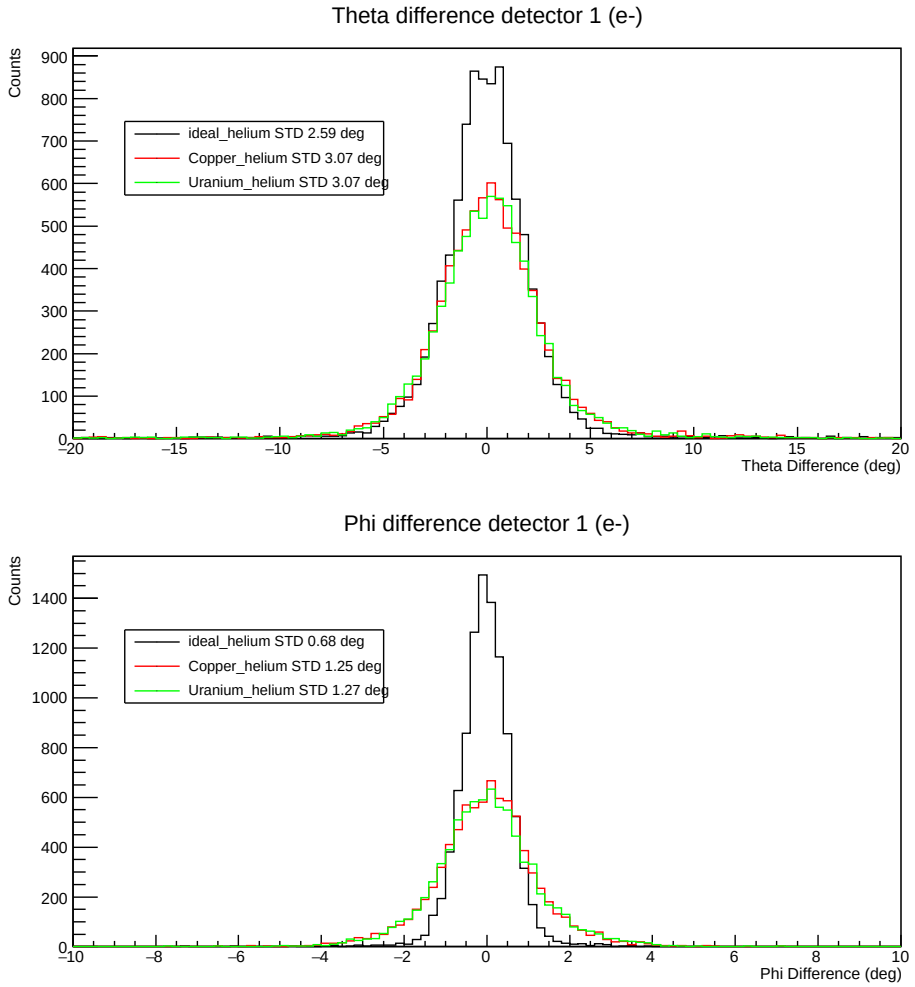

Figure 21: Comparison of the angular resolutions obtained with a 0.1 mm copper target and a 0.025 mm uranium target.

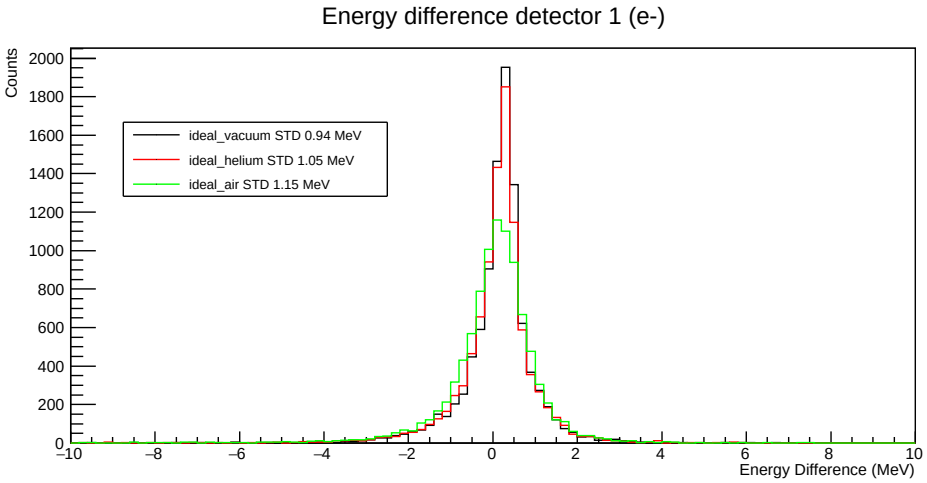

Figure 22: Comparison of the energy resolutions obtainable for electrons on detector package 1, with an "ideal" target for three different gas environments.

For the 0.025 mm Uranium target, the raw coincidence rate would be about 4 kHz, and the after cut rate about 80 Hz. For the 0.1 mm Copper target, raw coincidence rate would be about 500 Hz, and the after cut rate about 7 Hz.

These are not unreasonable count rates. We will have some ability to adjust rates by adjusting the beam intensity.

12 Helium Bag or Air

In all the above simulations we have assumed that the background environment is helium. i.e. the space through which the electrons and positrons move is filled with helium at atmospheric pressure. Between the target and this volume, and between the the helium volume and the VDCs there is a polyethylene bag to contain the helium.

To simplify construction of the magnet/detector system we now investigate whether this helium bag is actually necessary.

We first ran the simulation with an "ideal" target. "Ideal" refers to a fake (vacuum) target and a beam with no size. In each of the "Ideal" plots three scenarios are shown. 1. With no air or helium in the environment (i.e. a vacuum). 2. with a helium bag, contained by a polyethylene bag. 3. No bag and air in the environment. As examples, figure 22 shows how the energy resolution for electrons depends on these three scenarios, and figure 23 shows how the angular resolution for positrons depends on these three scenarios.

The difference between air and helium is clearly seen with helium being closer to a vacuum situation. This would suggest that helium would be the better choice over air. However, when we make the same comparison using a "real" target, with a finite beam spot size, the difference between helium and air is not so clear. As examples we show the comparison between when an air or helium gas is used in figures 24 and 25. The difference between air

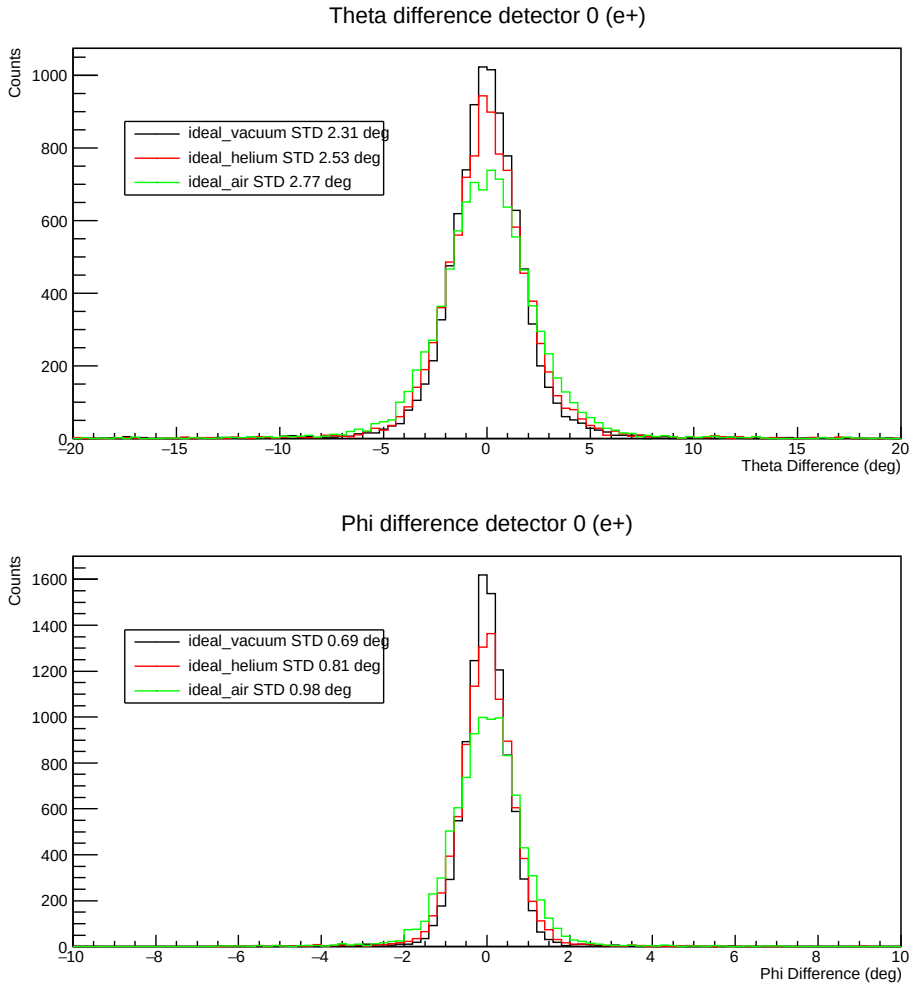

Figure 23: Comparison of the angular resolutions obtainable for positrons on detector package 0, with an "ideal" target for three different gas environments.

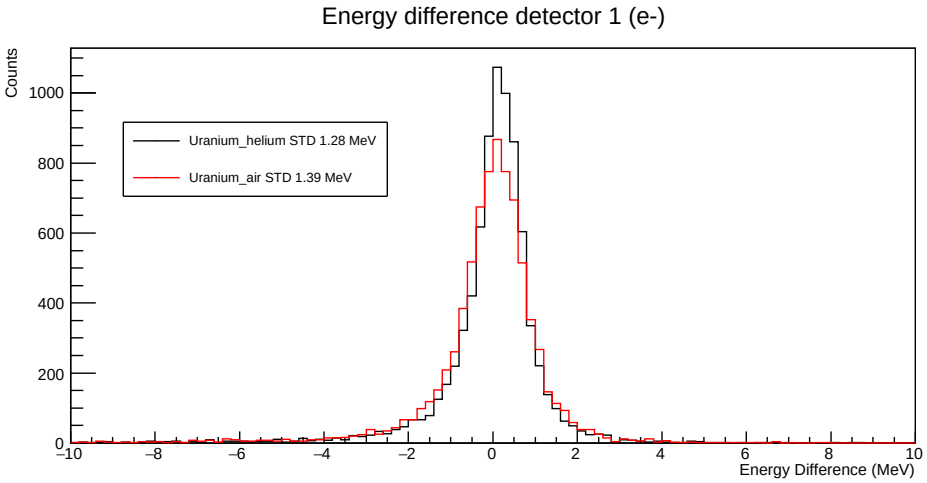

Figure 24: Comparison of the energy resolutions obtainable for electrons on detector package 1, with a uranium target for when a helium or air environment is used.

and helium is washed out by the multiple scattering in the target itself. This is confirmed with the copper target as well. Also shown in figures 26 and 27 are the comparisons for the polar and azimuthal angles for electrons and positrons.

Therefore our conclusion is that we can live without the helium bag without reducing the resolution beyond the limitations imposed by a finite thickness target. This significantly simplifies the experimental arrangement.

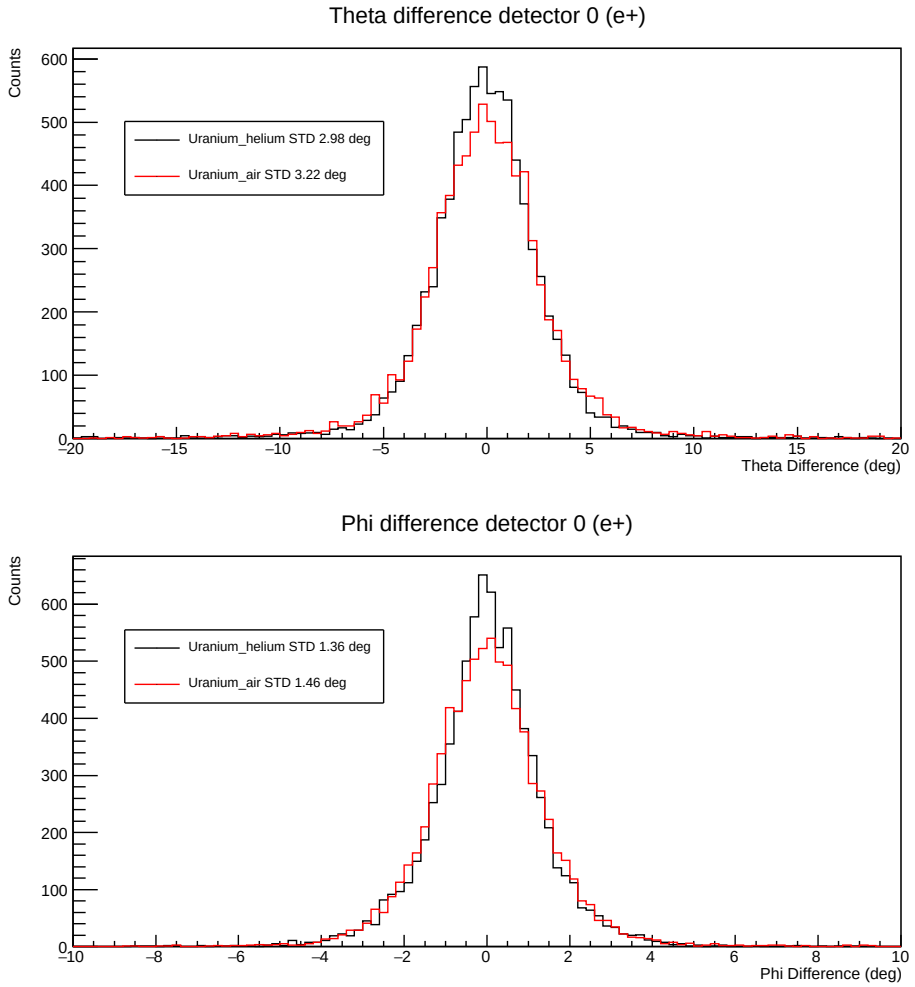

Figure 25: Comparison of the angular resolutions obtainable for positrons on detector package 0, with a uranium target for when a helium or air environment is used.

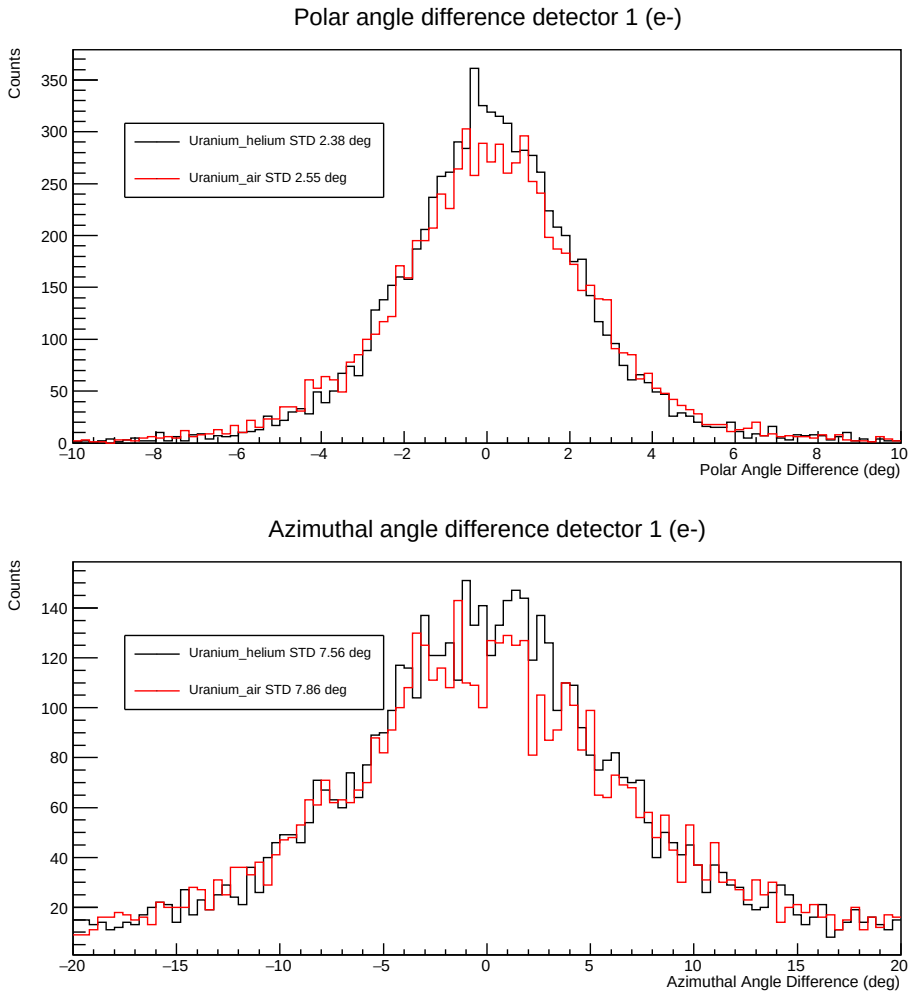

Figure 26: Comparison of the polar and azimuthal angular resolutions obtainable for electrons on detector package 1, with a uranium target for when a helium or air environment is used.

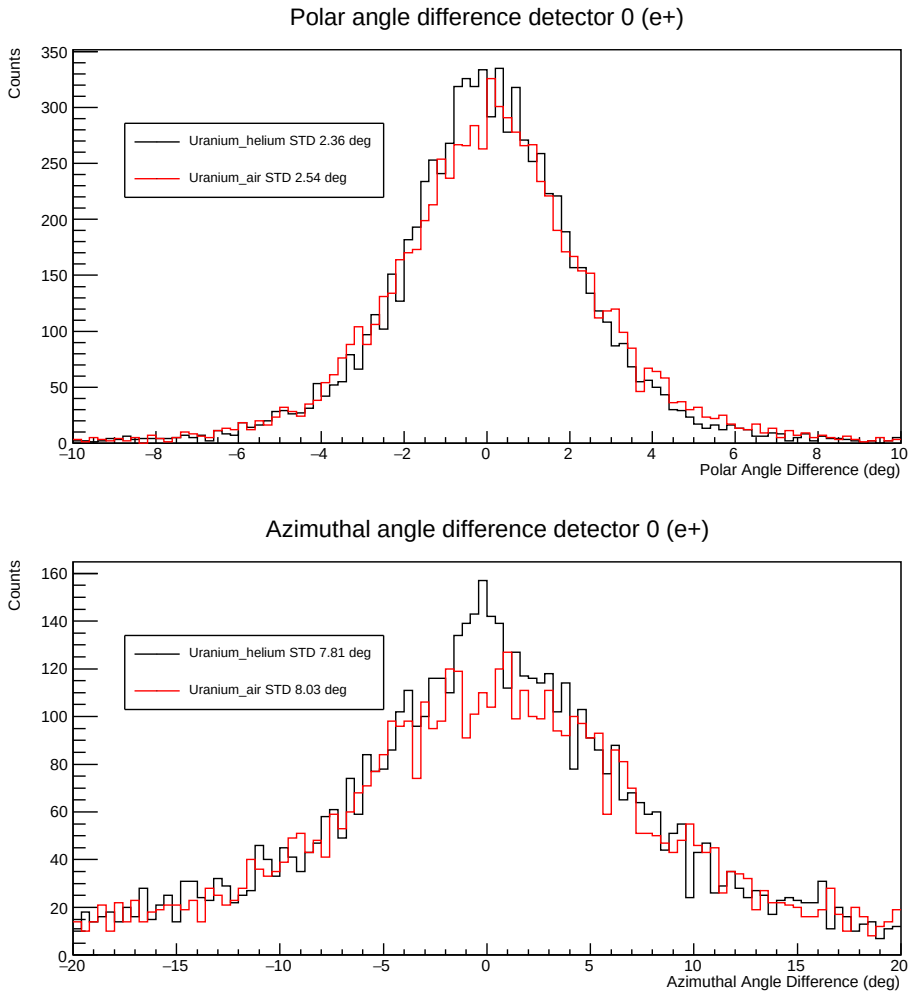

Figure 27: Comparison of the polar and azimuthal angular resolutions obtainable for positrons on detector package 0, with a uranium target for when a helium or air environment is used.

13 Increasing the Angular Acceptance.

As mentioned in section 4 the angular acceptance of the spectrometer is limited by the hole in the magnet yoke. It may be possible to increase the angular acceptance by moving the target postion forward (downstream).

The way the simulation was set up it was not possible to move the target postion forward very much and certainly not past the yoke entrance. Therefore modification were made to the code to allow investigations on the effect of moving the target.

Moving the target forward (downstream) does increase the the maximum horizontal angle (θ_i) of electrons or positrons that can pass through the hole in the yoke. The maximum vertical angle (ϕ_i) does not change much since that is limited by the pole gap.

It turns out that the more extreme angles, allowed by moving the target forward, means that the trajectory of some of those particles are passing very close to the edge of the circular pole of the magnet. In fact such particles are moving solely in the fringe field of the magnet rather than the more uniform central field. This introduces severe non-linearities in the transfer function between the energy and angle at the target and the positions and angles on the VDC. Introducing yet more higher order terms in the transfer function might be able to model this but, frankly I do not trust the simulation to that level of accuracy. (Recall that the magnetic field is described by a parameterization based on the limited field map measurements we have.) Another issue is that many of these more extreme angle particles never even make it to the detector. A hit on a detector requires that there be a hit in the hodoscope along with hits in both VDC layers.

Therefore only a modest movement of the target forward is possible. The design we have been working with up to now has a target distance (defined as the distance from the center of the circular magnet pole to the target) of 422.6 mm. This position means that the most extreme angles accepted are between 12° and 17° depending on where, within the beam spot (assuming a 1/2 inch diameter beam spot), the the source particle starts from. The median angle is about 14.7 deg.

We first investigate the gain in angular acceptance we do achieve by moving the target forward. We first run the simulation for a range of vertical angles ϕ_i ($\pm$2.5 mrad) for three target position distances. We run 10000 events and simply plot the number of events that hit the detector. (A detector hit is defined as infomation in the VDCs as well as a hit on the hodoscope.) We use a Uranium target. The range of horizontal angles simulated is not changed in each run. Figure 28 shows that there is not much difference in the vertical angle acceptance when the target is moved forward 2 cm.

We run the simulation for a range of positive and negative horizontal angles θ_i ($\pm$5 mrad) for three target position distances. Again we use a Uranium target, and the range of verical angles simulated is not changed in each run.

Figures 29 and 30 show that there is considerable drop off in acceptance as we go to larger θ_i angle (positive or negative). However there is a some gain in acceptance as we move the target forward. On average we increase the horizontal angular acceptance by about 40 mrad (2.3°). The agrees with the result from a purely geometric calculation which considers only the angles that can make it through the hole in the yoke.

Note that there is no benefit to moving the target forward if we are only intested in

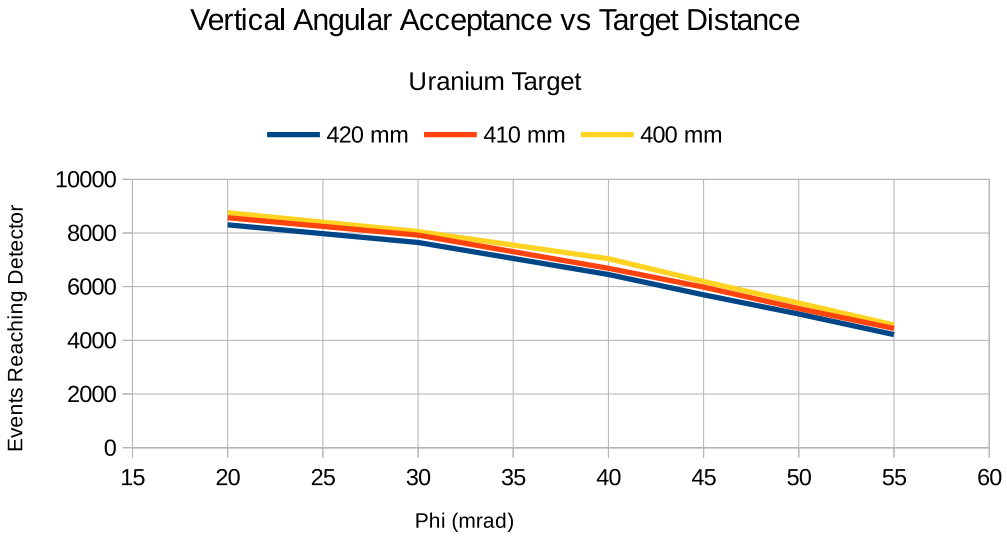

Figure 28: The number of events reaching the detector, when 10000 electrons are simulated, as a fuction of vertical angle and target position.

opening angles less than about 220 mrad (12.6°).

What is not clear from this is whether the transfer function relating the VDC information to the target energy and angles can be fitted with sufficient accuracy to preserve the resolution.

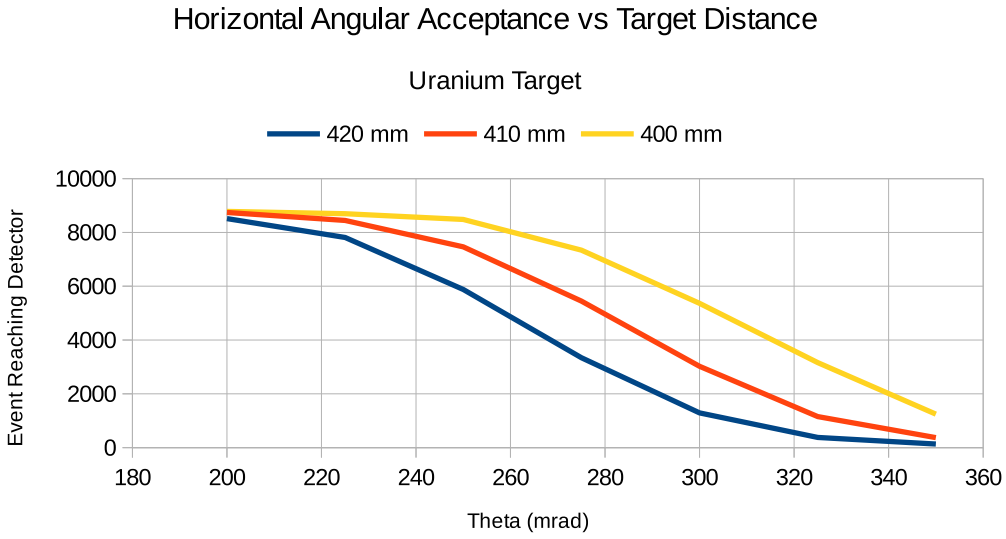

Figure 29: The number of events reaching the detector, when 10000 electrons are simulated, as a fuction of horizontal angle and target position.

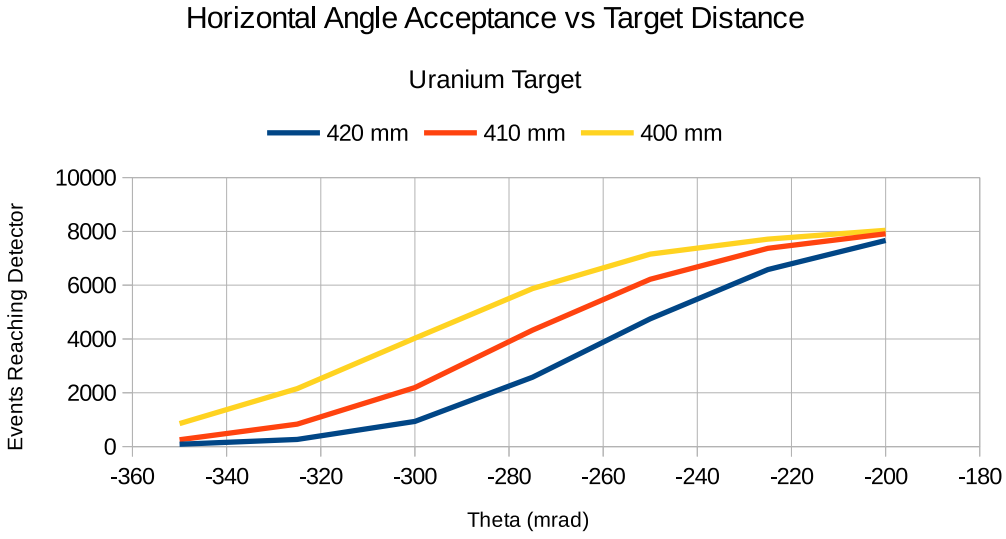

Figure 30: The number of events reaching the detector, when 10000 electrons are simulated, as a fuction of horizontal angle and target position.

References

[1] A Measurement of the Bethe-Heitler Pair Production Asymmetries. Proposal to the HIGS PAC-12. G. Ron *et al.*

[2] Field map obtained from B. Norum. Measured at JLab 5/7/2012.

[3] S. Kowalski and H.A. Enge, RAYTRACE, MIT, May 16,1986

[4] https://userweb.jlab.org/ brads/bethe-heitler/Qweak_R3_Chambers/

[5] John Leckey, Ph.D. Dissertation, College of William and Mary, 2012